Tailoring Secondary Interactions to Influence H-π versus n-σ* Competition in Hydrogen Bonded Complexes: A Matrix Isolation and *Ab Initio* Study

Priyanka Bansal

MS13116

A dissertation submitted for the partial fulfilment of

BS-MS dual degree in Science

Indian Institute of Science Education and Research Mohali

April 2018

Certificate of Examination

This is to certify that the dissertation titled "Tailoring Secondary Interactions to Influence H-π versus n-σ* Competition in Hydrogen Bonded Complexes: A Matrix Isolation and *Ab Initio* Study" submitted by Ms. Priyanka Bansal (Reg.No.MS13116) for the partial fulfilment of BS-MS dual degree programme of the institute, has been examined by the thesis committee duly appointed by the institute. The committee finds the work done by the candidate satisfactory and recommends that the report be accepted.

Dr.Arijit Kumar De Dr.SugumarVenkataramani Dr. P. Balanarayan

Prof. K.S. Viswanathan
(Supervisor)

Dated: April 20, 2018

Declaration

The work presented in this dissertation has been carried out by me with Prof. K.S. Viswanathan at the Indian Institute of Science Education and Research Mohali.

This work has not been submitted in part or in full for a degree, a diploma, or a fellowship to any other university or institute. Whenever contributions of others are involved, every effort is made to indicate this clearly, with due acknowledgement of collaborative research and discussions. This thesis is a bonafide record of original work done by me and all sources listed within have been detailed in the bibliography.

Priyanka Bansal
(Candidate)

Dated: April 20, 2018

In my capacity as the supervisor of the candidate's project work, I certify that the above statements by the candidate are true to the best of my knowledge.

Prof. K.S. Viswanathan
(Supervisor)

Acknowledgements

I would like to express my special thanks to my supervisor Prof. K.S. Viswanathan. I thank him for his continuous encouragement throughout the project which not only helped me to grow as a researcher, but also as a person. His advice on both research as well as on my career have been priceless.

I am deeply thankful to my committee members Dr. Arijit Kumar De, Dr. P. Balanarayan and Dr. Sugumar Venkataramani for their insightful comments and suggestions during my project work. I would like to thank Prof. D.P. Sarkar, Director, and Prof. N. Sathyamurthy, former Director, IISER Mohali, for supporting me with all the facilities. I gratefully acknowledge DST for awarding me the INSPIRE scholarship for pursuing my BS-MS degree.

I owe my special thanks to Dr. Ginny Karir for being an amazing mentor, a friend and a colleague. I am very thankful to her, for always being there whenever I had any questions and for all the help she provided to complete my thesis. With her even the proofreading process for the thesis was fun. Without her guidance and discussions, the thesis would not have come to a successful completion.

I sincerely admire Mr. Pravesh for helping me in synthesis, which would otherwise have been an impossible task for me. I am also very thankful to Dr. Ramashastry's lab for providing me D_2O for the experiments. I really appreciate my lab members, Dr. Anamika, Dr. Kanupriya, Jyoti, Pankaj, Divita and Amala for being very helpful and for maintaining a learning environment in the lab.

My hostel life was always fun with my best friend Pratibha. I owe my special thanks to Amit for always being there, and always been funny. I owe both of them a lot, for always supporting me, tolerating me. All the sleepless nights spent together, not studying and still consoling each other that we will do good in exams, gossiping, hunting for food everywhere but still end up going to hostel-5 canteen and eating Aaloo jeera are just few of the beautiful memories which I will cherish throughout my life. They are the reason for making my life so much easy and fun for all these five years. All this helped me completion of my thesis happily. I am also thankful to Mayank Saraswat for his comments and suggestions during thesis work.

Last but not the least, I would like to thank my parents, Mr. Rajesh Kumar Bansal and Mrs. Poonam Bansal for their endless support. I also thank my sister Supriya and my brother Rishab who were always very supportive and provided me with a lively and humourous environment over years. I thank my aunts, Mrs. Anu Aggarwal and Mrs. Shalini Aggarwal and my uncle, Mr. Rajiv Aggarwal for supporting me. Without all of them, I most certainly would not be where I am today.

Contents

List of Figures

List of Tables

List of Abbreviations

2,6-DCPhAc	2,6-Dichlorophenylacetylene
PhAc	Phenylacetylene
Ac	Acetylene
FTIR	Fourier Transform Infrared
TLC	Thin Layer Chromatography
SP	Stationary Point
Elec	Electrostatic
Dis	Dispersive
Pol	Polarization
Ind	Inductive
Rep	Repulsive
UV	Ultra Violet
GM	Gifford-McMahon
KBr	Potassium Bromide
HF	Hartree-Fock
MP	Møller–Plesset perturbation theory
DFT	Density Functional Theorem
CC	Coupled cluster
SCF	Self- Consistent Field
M06	Minnesota functional
FWHM	Full width at half maximum
ZPE	Zero point energy
CBS	Complete Basis Set
BSSE	Basis Set Superposition Error
AIM	Atoms-in-molecules
CP	Critical point
NBO	Natural Bond Orbital
LMOEDA	Localized Molecular Orbital Energy Decomposition Analysis

Abstract

Hydrogen bonded complexes of 2,6-dichlorophenylacetylene (2,6-DCPhAc) with H_2O were studied experimentally using Matrix Isolation Infrared Spectroscopy, and corroborated through *ab initio* computations. The question addressed in this thesis concerns the competition between H-π and n-σ* hydrogen bonded structures in phenylacetylene systems with H_2O and the factors that govern the relative stability of the two isomers.

It was shown earlier that while in Acetylene (Ac)-H_2O complex, Ac served as the proton donor, forming the n-σ* complex, the PhAc-H_2O system manifested a H-π structure, where H_2O was the proton donor to the acetylenic π cloud of PhAc. The switch in roles was attributed to the presence of a secondary contact involving a hydrogen bonding interaction between the aromatic C-H of PhAc and the oxygen of H_2O (i.e. C-H···O interaction). The question asked here is the following: If the C-H group involved in the secondary interaction is replaced with a C-Cl group, thereby suppressing the C-H···O interaction, would there be a change in the relative stability of the H-π and n-σ*isomers? Towards finding an answer to the above question, hydrogen bonding interactions in 2,6-DCPhAc-H_2O system was studied.

Ab initio computations were performed using M06-2X and MP2 methods with 6-311++g** and aug-cc-pVDZ basis sets, using Gaussian-09 software. Interaction energies of the complexes were also computed using single point calculations at the CCSD(T) level at the CBS limits. Frequency calculations were performed to assign our experimental features and to confirm if the structure corresponding to a stationary point is a minimum. AIM and NBO calculations were done to understand the nature of the interactions in the complexes. Calculations showed that the energy gap between the H-π and n-σ* isomers in the chloro derivative is smaller than in the unsubstituted PhAc-H_2O system; pointing to the loss of stabilization of the H-π complex relative to the n-σ* structure in the chloro system. At the MP2/aug-cc-pVDZ level, BSSE corrected interaction energies actually show a flipping of the relative energies of the complexes, indicating the n-σ* complex to be more stable than the H-π isomer. Matrix isolation experiments also confirmed the presence of the n-σ* structure in the matrix. This work has therefore highlighted the important role of the secondary interaction, alluded to in the earlier work. This work has also highlighted that by suitably tailoring the structure of the precursor molecules, one can tune the competition between nearly degenerate structures.

Chapter1

Introduction

Non-covalent interactions are all pervasive and form a very important part of structural chemistry, biochemistry and supramolecular chemistry.[1] These weak interactions dictates the shape of many large biological molecules, drives spontaneous folding of proteins and nucleic acids. These interactions though weak often times determine the architecture of supermolecules in supramolecular chemistry. These are some of the reasons which make the study of non covalent interactions important. The non-covalent interactions are remarkably different from the stronger covalent interactions in terms of nature and as well their role in bonding. Hobza *et al.* describe in their book, non-covalent interactions are considerably weaker than covalent bonds but despite, or probably because of this, non-covalent bonds play a subtle but decisive key role in nature.[2],[3] The hydrogen bond is one of the most important non-covalent interaction which has been described in the next section.[4,5]

1.1 The Hydrogen Bond

The concept of hydrogen bond has now been known for over a century but it still holds paramount importance in all fields of science. It is important in many chemical processes and its importance in biological systems is unquestionable. Hydrogen bonding is the most significant non-covalent interaction responsible for the unique solvent properties of water. It determines protein structure by zipping the molecule into a particular three dimensional shape which is crucial for deciding function of a protein. It is also responsible for holding the strands of DNA together. Hydrogen bonds are also important in supramolecular chemistry for designing molecules with desired properties.[6] These are only a few reasons which reflect why it is important to study hydrogen bonds.

The very first observation of what today is known to be a hydrogen bond, was in the year 1902.[6] It was later followed by few more such reports. In 1912, Moore and Winmill were the first ones to report hydrogen bond in organic chemistry and they used the term weak union to describe the basic properties of trimethylammonium hydroxide in comparison with tetramethylammonium hydroxide.[7] Later in 1920, Latimer and Rodebush while referring to the structure of trimethylammonium hydroxide suggested the hydrogen bond as “a pair of electrons on one water molecule might be able to exert sufficient force on hydrogen held by a

pair to electrons on another water molecule to bind two molecules together" and that "the hydrogen nucleus held between two octets constitutes a weak bond".[8] It was not until 1939, when Pauling first used the term *hydrogen bond* to account for the residual entropy of hydrogen bond. Pauling described hydrogen bond to be electrostatic in nature, and this understanding limited the hydrogen bonds to be only present when the hydrogen is attached to a highly electronegative atom (N,F and O).In 1960, Pimental and McClellan addressed the limitation of the Pauling's definition of hydrogen bond and took into account the possible hydrogen bonding interaction that can exist with groups such as C-H, P-H, and of π-acceptor, and many other groups.[9,10]

1.2 Definition of the hydrogen bond

In order to account for the recent experimental and theoretical findings for hydrogen bonding interactions, a task group formed by International Union of Pure and Applied Chemistry [11] proposed a modern definition of the hydrogen bond 2011 as follows:

"The hydrogen bond is an attractive interaction between a hydrogen atom from a molecule or a molecular fragment X-H in which X is more electronegative than H, and an atom of a group of atoms in the same or different molecule, in which there is an evidence of bond formation."

A hydrogen bond can be represented as X-H···Y-Z, where X-H acts as the hydrogen bond donor. The hydrogen bond acceptor can be an atom or an anion Y, a molecular fragment of the molecule Y-Z itself. The hydrogen bond can exist even when X and Y are same, such that X-H and Y-H distances are also same leading to formation of a symmetric hydrogen bond. The acceptor represents electron rich region, can be anything ranging from very electronegative atoms to a lone pair or even a π-bond pair. The modern definition takes into account a number of donors and acceptors possible that can involve in hydrogen bonding, therefore also taking into consideration the formation of a weak hydrogen bond where either of donor or acceptor, or both of them have moderate or low electronegativities.

The book by Desiraju and Steiner defines the weak hydrogen bond as an interaction X-H···A wherein a hydrogen atom forms a bond between two structural moieties X and A, of which one or even both are only of moderate to low electronegativity.

The energy of a hydrogen bond typically ranges from -0.5 kcal/mol to -40 kcal/mol.[12] A range of criteria are used to distinguish very strong, strong and weak

hydrogen bonds and one such method is on the basis of their bond energies. The bond energy values for very strong bonds lie in the range of -15 to -40 kcal/mol as observed in $[F\cdots H\cdots F]^{-}$, $[N\cdots H\cdots N]^{+}$. Strong bonds like O-H···O=C, N-H···O=C, have bond energies ranging from -4 to -15 kcal/mol and energy of weak bonds lies typically between -2 to -4 kcal/mol. The weak bonds can form between weak donors and strong acceptors as in C-H···O/N or between strong donors like O-H and weak acceptors like C≡C, phenyl π cloud etc. A weak hydrogen bond can also form between weak donors and weak acceptors and some of the examples include C-H···π, C-H···F-C etc. The weak hydrogen bonds are associated with small binding energies which allow fast rearrangements at certain temperatures, hence making their study important both in the field of chemistry and biology.[13]

The C-H bond is a weak hydrogen bond donor and as described in Desiraju's book, the hydrogen donor propensity of C-H bonds is C(sp)-H> $C(sp^2)$-H > $C(sp^3)$-H and increases with the number of adjacent electron withdrawing groups. Also, the C-H···π interactions are often regarded as the weakest class of hydrogen bonds with dispersion interactions being the major source for attraction in formation of the hydrogen bond.

1.3 Methods to study hydrogen bonds

1.3.1 Crystallography

Diffraction methods are used to study weak hydrogen bonds which are otherwise a challenge to study. Crystallographic techniques helps to determine the three dimensional structure of molecules to atomic resolution. X-ray diffraction serves as an important tool for determination of position of hydrogen atoms which is based on the principle of interaction of X-rays with the electron density of the molecule under consideration. Neutron diffraction serves as a more accurate method for determining the position of hydrogen atoms, where neutrons interact with the nuclei of the atoms.

1.3.2 Spectroscopic studies

Vibrational spectroscopy is a method widely used as a probe to study all kinds of hydrogen bonds. Whenever there is a formation of a hydrogen bond, there occurs many prominent changes in the vibrational spectra of the molecules involved depending upon the strength of interaction involved between them. These changes are nothing but the frequency shifts that occur upon complex formation depending on the strength of hydrogen bond formed. When a 'proper' hydrogen bond forms between X-H and Y, there can be lengthening

of the X-H bond and weakening of bond due to transfer of electron density from proton acceptor to proton donor which causes both a red shift and increase in its intensity in the IR spectrum. There can also be cases where X-H bond contracts, causing a blue shift and decrease in intensity in the IR spectrum, commonly known as improper hydrogen bonds.[14] Gas-phase rotational spectroscopy is also used to study the hydrogen bonded adducts corresponding to global minimum. These studies also helps to obtain various other parameters of paramount importance like dissociation energies, force constants, geometries, which are otherwise not possible to obtain with the experiments in condensed phase.

1.3.3 Computational studies

Theoretical insights that advance our understanding of hydrogen bonding can be afforded by employing various computational methods. Experimental methods listed above gives us the information regarding the geometry of molecules. On the other hand, computational methodologies can be used to study potential energy surface which is important to understand the interconversion happening between various geometries. The computational studies also provide a detailed information regarding the interaction energies without any complications due to solid state or solution environment and also on nature of interaction involved. Above all, the theoretical studies are necessary to support the experimental results obtained.

1.4 Motivation

It is interesting to study the molecules which offer multiple hydrogen bonding sites, especially when these sites are equally competitive in terms of weak non covalent interactions. To illustrate how there exists a hydrogen bonding competition among various sites in multifunctional molecules, a few examples are listed. Propargyl alcohol acts as a multifunctional molecule, it can act as a proton donor through acetylenic C-H and O-H sites. It can also act as a proton donor through O atom and π electron cloud. Hence, when it involves in hydrogen bonding, there exists a competition whether it will act as a proton donor or a proton acceptor. In addition to this, there is also a competition among various proton donor and proton acceptor sites.[15,16] PhAc and Ac are typical the examples of systems offering the competitive interplay between various donor acceptor sites for hydrogen bonding. In Ac, there are two hydrogen bonding sites, the acetylenic C≡C π-cloud which acts as a proton acceptor site and acetylenic C-H group which acts as a proton donor site. In

PhAc, in addition to the hydrogen bonding sites on acetylene moiety, a phenyl π-cloud which acts as a proton acceptor site is also present. Given such a rich landscape, there are a number of structures possible when these molecules form a hydrogen bonded heterodimers with H_2O, which in itself is an amphiprotic molecule. Similarly, 2,6-DCPhAc is also a multifunctional molecule in terms of hydrogen bonding sites as shown in Fig. 1.1.

The competition between these interaction sites can sometimes be unpredictable. To exemplify it take the case of hydrogen bonded complexes of Ac with H_2O. Computational studies indicated only two possible structures for Ac-H_2O system. One of the structures involved an O-H···π interaction where acetylenic π cloud acts as proton acceptor with water, forming a H-π complex and the other structure involved a (C-H···O) interaction in which water acts as the proton acceptor from the acetylenic hydrogen, forming a n-σ* complex. The latter structure was shown to be the global minimum. Engdahl *et. al*[17] studied the hydrogen bonding interactions in Ac and H_2O, using matrix isolation infrared spectroscopy and they observed the n-σ* complex in the matrix experiments which is also expected based on the relative gas phase acidity values.[18] The PhAc-H_2O system has been studied using gas phase microwave spectroscopy and IR-UV double resonance spectroscopy. Both studies observed the O-H¨π complex, and which was shown to manifest a cyclic quasi planar structure and which turned out to be the global minimum involving (O-H···π) and (C-H···O) interactions. The n-σ* structure which was the global minimum in Ac-H_2O system was not at all observed in these experiments. In order to comprehend the hydrogen bonding behaviour of PhAc-H_2O system, Karir *et. al*[19] studied the hydrogen bonded complexes of PhAc and H_2O using matrix isolation FTIR spectroscopy. In their experiments they indeed observed n-σ* which was a local minima. Unfortunately H-π complex could not be observed in their experiments due to spectral interferences. In their study, Karir *et al*. also addressed the question as to why there occurs a role reversal in PhAc-H_2O system, i.e. why in the PhAc-H_2O system the n-σ* complex is not a global minimum as predicted by the gas phase acidity values, but rather it is the H-π complex which is the more strongly bound complex. The reason attributed to this role reversal was the presence of an additional (C-H···O) secondary interaction in PhAc-H_2O system which is not manifested in Ac-H_2O system. Hence, it is the team play of the acidities and the secondary interactions which

decides who wins in the H-π and n-σ* competition. The focus of this thesis is tailoring secondary interactions to influence the H-π versus n-σ* competition in hydrogen bonded complexes using 2,6-DCPhAc-H_2O complexes as model system.

Tailoring of secondary interactions can be done by substituting the C-H group with some other group that may suppress the (C-H···O) interaction. The two equivalent C-H groups on benzene ring in PhAc are replaced by C-Cl groups, thereby suppressing the (C-H···O) interaction. The primary motivation for this work is to address the following question: What would be the change in relative stabilities of n-σ* and H-π isomers when the secondary interaction site playing a decisive role in determining the global minimum in PhAc-H_2O system is replaced by C-Cl group. Therefore, in this study, we examined the hydrogen bonding interactions of 2,6-dichlorophenylacetylene (2,6-DCPhAc) with H_2O, both experimentally and computationally.

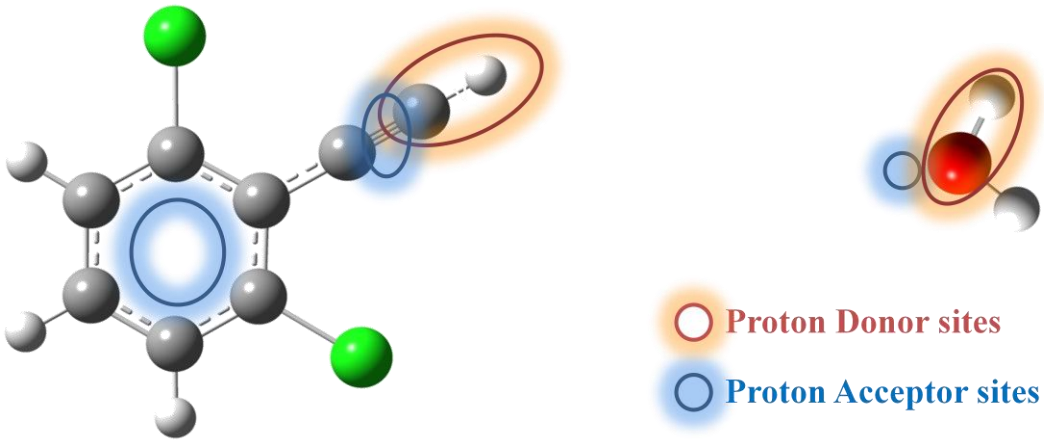

Figure 1.1 Hydrogen bonding sites in 2,6-DCPhAc and H_2O molecules.

Chapter 2

Experimental and Computational Methods

2.1 What is Matrix Isolation?

The term 'matrix isolation' was coined by George Pimentel[20] and George Porter[21] and refers to chemistry occurring in cages at very low temperatures. This technique involves trapping of guest molecules of interest in large excess of inert gas such as Ar, N_2, Kr which serve as rigid matrices. The molecules of interest are deposited along with an inert gas on to a cold substrate mounted on a cryostat temperature of ~12 K to produce a thin solid film. The central idea of this is technique is to reduce the intermolecular interactions among the analyte molecules, leading to an uncongested spectra having small linewidths. The low temperatures (typically 4- 20K) prevents the occurrence of any process which has an activation energy of more than a few kJ mol^{-1}. This technique offers various advantages when it comes to studying the unstable molecules having fleeting lifetimes such as radicals, carbocations, carboanions *etc*, and to study various types of weak non covalent interactions This technique also offers the possibility to study local minima along with the global minimum structures which is often not possible in gas phase spectroscopic studies.[22] The matrix isolation technique can be used in conjunction with a variety of spectroscopic tool to study the trapped species such as FT-IR, ESR[23], UV-Visible spectroscopy[24].

In order to serve as a matrix, the substance must have certain chemical and physical properties.[25] It should be chemically inert to the analyte molecules. The noble gases such as Ne, Ar and N_2 are very commonly used. We can also deliberately choose a material which is reactive towards the analyte species depending on the study under consideration. For example, CO and O_2 can be used to trap various reactive species like carbenes.[26] The matrix material should be sufficiently rigid at the temperature of the experiment, to prevent the diffusion of analyte species, and it must be suitable for accommodating them in lattice sites in the matrix. Transparency is yet another important factor to ensure that the matrix should not show any absorption in the spectral region of interest. The matrix gas, along with sample molecules is deposited on to a cold window. Again, the choice of window depends on the type of spectroscopy one wants to use. KBr, NaCl (transparency in region 400 – 4000 cm^{-1}), CsI and CsBr (transparency in region < 400 cm^{-1}) windows can be used for IR studies.

Quartz and copper or sapphire windows can be used for UV- visible and EPR spectroscopy respectively. A general guideline that is followed to ensure the rigidity of the matrix is to keep the temperature of the cold window at 30% below melting point of matrix material used.

Matrix isolation technique is used to minimize the interactions between the analyte molecules by trapping them in a cage of a matrix. Even though the isolation of analyte molecules is achieved, their interactions with the matrix atoms cannot be ignored. These interactions are evident in the infrared spectra and can be attributed to a number of matrix effects. A cartoon description of the technique has been shown in Fig. 2.1.

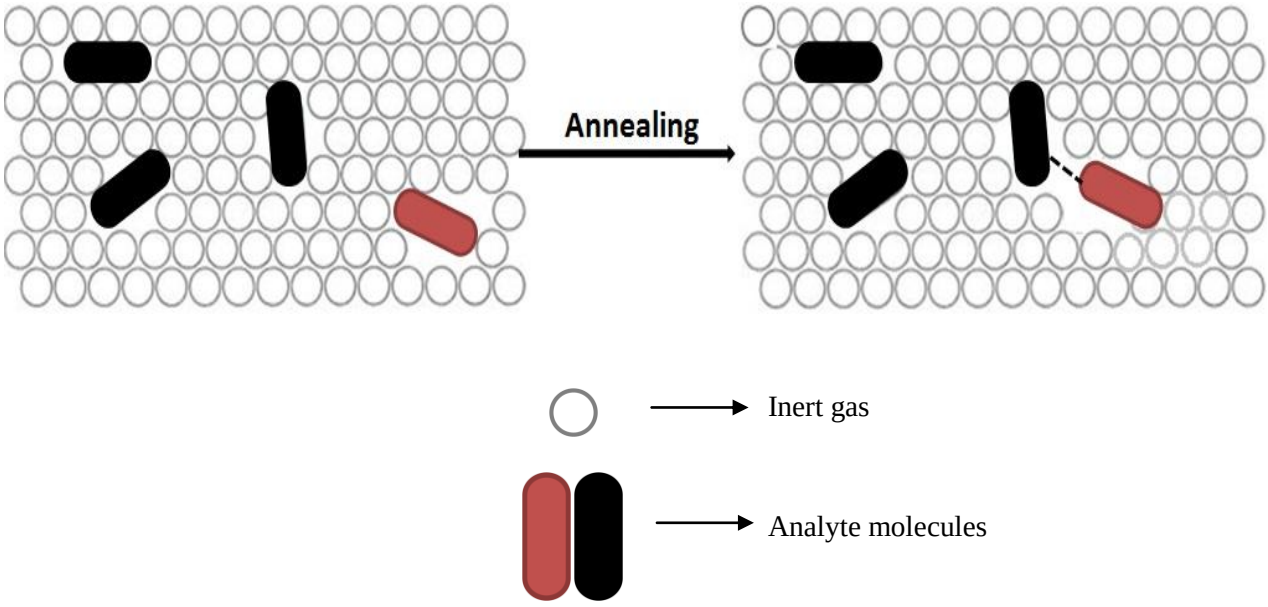

Figure 2.1 Cartoon describing the matrix isolation technique

2.2 Advantages and Disadvantages

The major advantage of using matrix isolation technique is that it provides reasonably uncongested spectra with sharp line widths of ~ 2-4 cm^{-1}. The isolated molecules in a rigid cage are devoid of any type of collisions, rotations and spectral congestion, thus enables one to obtain very sharp spectral linewidths as compared to the spectra obtained using other solid and liquid samples. The vibrational shifts observed for non-covalent interactions range from ~2 cm^{-1} for very weak hydrogen bonded complexes to ~800 cm^{-1} for very strong hydrogen bonded complexes.[27,28] These very small linewidths enables one to study small perturbations

in the infrared lines resulting from very weak intermolecular interactions, thereby offering a great advantage to study hydrogen bonding and van der Waals interactions.

There are various limitations associated with this technique. It can only be used to study those species which are volatile at reasonable temperatures, without decomposition. Hence, the sample is required to have a sufficient vapour pressure at attainable temperatures in order to be deposited on to a cold substrate. This rules out the possibility to study various interesting compounds such as biologically relevant molecules.

2.3 Solvation effects of Matrix

2.3.1 Matrix effects

It is important to understand the perturbation in the vibrational modes of the trapped species due their interaction with matrix atoms. The matrix environment influences vibrational spectra in a particular way and contains information about intermolecular forces by causing shift in the frequencies relative to isolated gas phase values, or forming multiplets instead of a single feature. The frequency shift, $\Delta\nu$, arises from electrostatic ($\Delta\nu_{elec}$) interactions, inductive ($\Delta\nu_{ind}$) interactions, long range dispersion ($\Delta\nu_{dis}$) and short range repulsive ($\Delta\nu_{rep}$) interactions and can be represented as:

$$\Delta\nu = \nu_{matrix} - \nu_{gas} = \Delta\nu_{elec} + \Delta\nu_{ind} + \Delta\nu_{dis} + \Delta\nu_{rep} \ldots\ldots.$$

The shift is a measure of the strength of the interactions. Usually, for noble gases, dispersive interactions and repulsion forces dominates. Pimental and Charles[29] have used Buckingham equation for a perturbation treatment to describe the effect of a solvent environment on the vibrational frequencies of a diatomic molecule given by:

$$\nu_{matrix} - \nu_{gas} = \frac{B_e}{hcw_e}\left[U'' - 3\frac{A}{w_e}U'\right]$$

$B_e = h/8\pi^2 m_r c\, r_e^2$ is the rotational constatnt,

A = Aharmonicity constant

U = Energy due to solute-solvent interactions

$U' = \{\partial U/\partial r_{BC}\}$ and $U' = \{\partial U^2/\partial^2 r_{BC}\}$, r_{BC} = equilibrium distance between and C of molecule ABC as shown in Fig. 2.2.

cw_e = Harmonic oscillator frequency

In the Fig. 2.2, 'ABC' represents a triatomic molecule trapped inside a matrix cage and the matrix atom 'M' is the nearest neighbour to C. The matrix cage effect on U, U' and

U'' can be determined from the figure using Buckingham's expression. In a tight cage, where the distance between atoms C and M, R_{CM} is less than R_e ($R_{CM} < R_e$), suggests that U' and U'' are both positive. This implies a positive value of $\Delta\nu$ and therefore a blue shift. For a loose cage, where $R_{CM} > R_e$, leads to negative values for both U' and U''. This means that $\Delta\nu$ is negative and hence suggesting a red shift. This result can be generalized for the polyatomic molecules as well. Therefore, a high frequency mode in a polyatomic molecule such as stretching modes being small amplitude modes imitates a loose cage and suffers a red shift. On the other hand, the low frequency modes which have very high amplitude, like bending mode, resemble a tight cage and show a blue shift. Understanding analyte-matrix interactions makes the vibrational mode assignment and interpretation of the spectra easy.

Besides frequency shifts, it is common to observe multiplet features in the spectra. This effect can be attributed to aggregation, rotation of an analyte in the matrix cage and presence of multiple trapping sites. These are discussed in detail in the following section.

2.3.2 Multiple trapping sites

The matrix gas adopts a particular lattice structure on solidifying depending on the matrix gas used. N_2 adopts a face centered cubic (fcc) and Ar adopts a hexagonal close packed (hcp) structure. The interstitial and substitutional sites act as potential trapping sites for the analyte molecules. All analyte molecules do not necessarily all get trapped in identical sites. Rather, they experience different environment, gets perturbed differently and induce slightly different shifts.

As a result, a multiplet structure is observed with intensities proportional to stability of each trapping sites which otherwise would have been a single intense peak. The multiplet features observed due to different matrix sites is termed as site effect. It is highly unlikely that the sites will be identical for different matrices, hence the features observed in the spectra due to site effects can be identified by changing the matrix gas. Also, on raising the temperature of the matrix, it is possible to get rid of unstable sites and consequently allowing for the multiplet features to reduce to produce sharp features.

2.3.3 Rotation of an analyte in matrix cage

Ideally, the trapped analyte molecules in an inert matrix cage at very low temperatures (4- 20K) are expected to be devoid of rotations. But in reality, the rotations are not completely absent. It is possible for some small molecules such as ammonia[30], water[31],

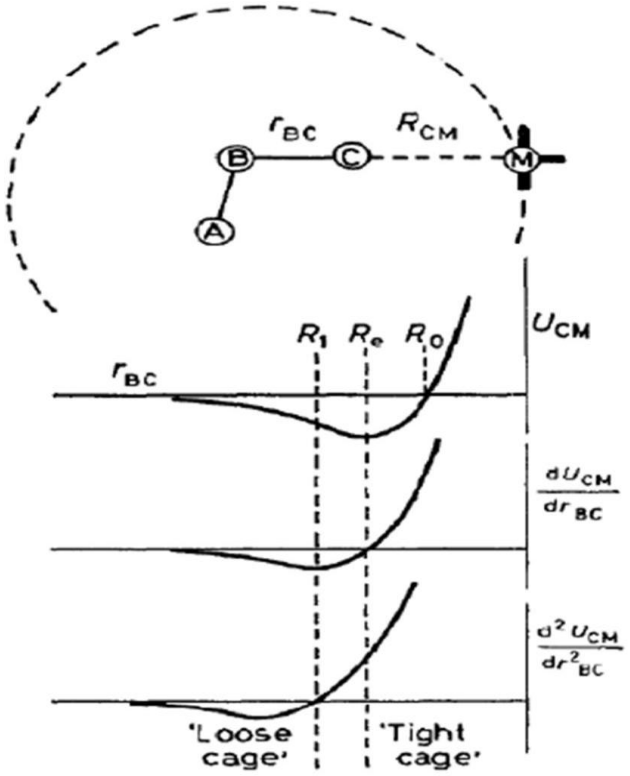

Figure 2.2 Plot showing the dependence of U, U' and U" on matrix cage

alkali halides etc.[32] to rotate in noble gas matrices having sufficiently large cavities and cause multiplet splitting. One such example is H_2 in a nitrogen matrix. Temperature cycling is employed to identify the features arising due to rotations. As temperature is varied, there occurs a population change in rotational energy levels leading to reversible intensity variation.

2.3.4 Aggregation

In an ideal matrix isolation experiment, it is always desired to ensure isolation of analyte molecules trapped in cage of matrix gas. Various factors that decide optimum isolation are the deposition rate, the deposition time and the matrix ratio. A very high degree of isolation can only be achieved at high matrix/analyte (M/A) ratios, usually greater than 1000: 1. At lower ratios, molecular aggregates get trapped in the matrix and induce many spectral effects such as broadening, slight shifts and sometimes multiplets. Hence it is important to determine the effects of varying concentrations of individual monomers to eliminate the spectral features arising due to formation of self aggregates. The probability of isolation for a molecule like CO occupying a single substitutional site can be calculated in

the following way. The probability of interaction is a chance of finding another molecule occupying one of the 12 sites that form the cage. Hence, the chance for the CO molecule not being present at those sites can be calculated as, $P = (1-r)^{12}$ given that 'r' is reciprocal of the matrix ratio. For very high matrix ratios i.e. very small value of 'r', the above expression reduces to $P = 1 - 12r$. This means that a matrix ratio of 1000 is required to ensure 99% isolation. Contrary to the result of this analysis, it has been found experimentally that various dimers, trimers and other higher aggregates of CO do form at same matrix ratios. Another such example is of lithium atoms which dimerize completely at even at matrix ratio of 10,000:1, unless the deposition rate is kept very fast. Therefore, the spectroscopic features due to well isolated monomer species needs to be distinguished from those due to aggregates by performing systematic variation of matrix ratio and by initiating diffusion by controlled warming of the matrix.

2.3.5 Lifting of degeneracy of vibrational levels

The symmetry of the site occupied by molecules can also induce matrix effects. The trapped molecule gets perturbed differently in different sites. For degenerate vibrational modes, the asymmetry of trapping site can lift the degeneracy, resulting in splitting of a vibrational mode and appearance of multiplet features. This effect has been observed for CO_2 and C_2H_2 in N_2 matrix. Between N_2 and Ar matrices, N_2 is is known to interact more strongly with the analyte molecules than Ar.

2.4 Matrix isolation infrared setup

The experimental setup combines the matrix isolation technique with infrared spectroscopy to unravel information about the vibrational features of the weakly bonded complexes. The apparatus used for these experiments include the following components:

1. Cryostat
2. Vacuum system
3. Sample Introduction Assembly
4. Fourier Transform Infrared (FTIR) Spectrometer

1. Cryostat

A cryostat is used to maintain very low temperatures such as ~12 K of the devices or samples which are mounted inside it. In our experiments, the KBr window mounted within the cryostat reaches a cryogenic temperature of ~12K using helium as a working fluid. It is a

closed cycle helium compressor cooled cryostat CH-202w/HC Model (Sumitomo Heavy Industries Ltd), which works on the principle of Grifford-McMohan (GM) refrigeration cycle. A typical closed cycle cryostat constitutes the following components: expander, compressor, vacuum shroud, and radiation shield. The Expander, also known as cold head of cold finger, is where the GM cycle takes place. It is linked to the compressor via two gas lines. One of the gas lines introduces high pressure helium gas to the expander, and other returns low pressure gas from the expander. A vacuum shroud is constructed using stainlesssteel or Aluminum which makes it less vulnerable to adsorbing water. The cold end of the expander is surrounded by the vacuum shroud to limit the heat load on the expander due to conduction and convection. Since cooling occurs in three stages, the radiation shield which is constructed using high purity copper insulates the second stage from room temperature thermal radiation emitted from the vacuum shroud. In addition to these components, several other support components are needed. A temperature controller (Lakeshore Instrumnets-Model 335) has been used to measure and adjusts the temperature of the sample deposited on the window. In addition to it, a chiller unit (3kW, Werner Finley) is needed to remove heat from the low pressure working fluid before returning to the compressor. Fig 2.3 shows a general schematic for a closed cycle cryocooler.[33] The cryostat and its associated units are shown in Fig. 2.4.

2. Vacuum System

High-vacuum pumps are neded for evacuation of the cryostat and sample preparation line. The key to study various molecular species using matrix isolation infrared spectroscopy is to attain very low temperature and very high vacuum conditions. A variety of pumps can be used to achieve the desired vacuum. In our experimental setup, we use diffusion pump (Edwards, Diffstak MK2 series 100/300), backed by a rotary pump (Hind Hivac; ED6) is used to attain a pressure of ~10^{-6}mbar. First a roughing vacuum is attained using a mechanical rotary pump with pumping speed of 200L/min from atmospheric pressure to ~10^{-3} mbar. It consists of a housing, vanes, an eccentrically installed rotor, an inlet and an outlet, a working chamber and an outlet valve. Air is drawn into the chamber through an inlet and is compressed until the outlet valve opens against the atmospheric pressure. Then a diffusion pump is employed to take down the pressure to ~10^{-6} mbar with pumping speed of 300 L/sec. It consists of a chamber housing an oil vessel, a heater, a chimney and a nozzle.

The chamber's outside surface is wound by cooling coils carrying water. The heater vaporizes the oil which rises into the vapour chimney, then get deflected downward by the nozzles and during this process imparts momentum to randomly moving gas molecules in the chamber. Hence, the momentum deflects the molecules in random direction towards the pump exit, thereby creating vacuum. The vacuum inside the system is measured using a Pirani Gauge 26 (Edwards APG 100 Active Pirani Gauge) and a digital Penning gauge (Hind Hivac) as shown in Fig. 2.5.

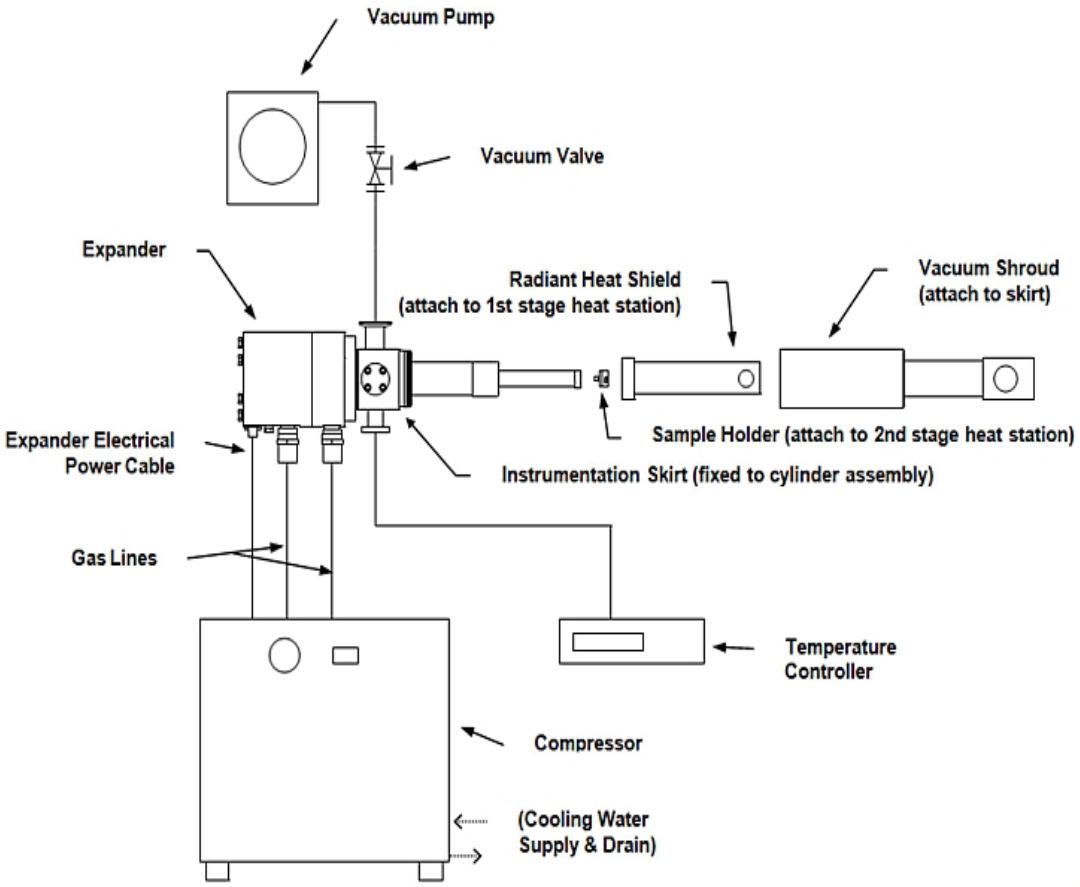

Figure 2.3 Closed cycle cryocooler set-up

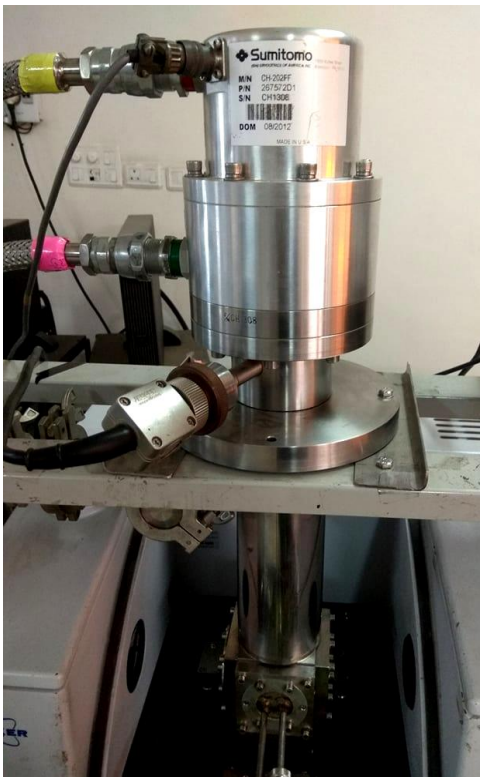

Cryostat

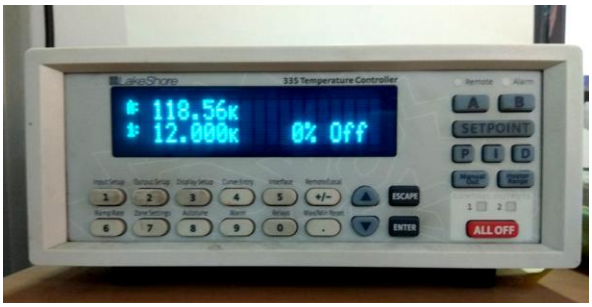

Temperature Controller

Helium Compressor

Figure 2.4 Cryostat and associated units

Figure 2.5 Diffusion pump

3. Sample Introduction Assembly

The method of depositing the sample on the substrate depends on the nature of the sample to be studied. Matrix isolation technique can only be used to study those species which are volatilizable without decomposition, therefore setting a limit on the size as well the thermal stability of the species to be studied. Once the temperature of the KBr window reaches 12 K and pressure of the system comes down to ~10^{-6} mbar, the sample molecules can be deposited. First, the sample/inert gas mixture is mixed in a 1 L stainless steel mixing chamber ensuring 1:1000 dilution. The sample was containted in a sample bottle and was introduced to the mixing chamber via one of the five ports on mixing chamber. A particular temperature of the sample is maintained so that it acquires optimum vapour pressure and then mixes well with the matrix gas. The compounds having low vapour pressure are heated whereas, the compounds with very high vapour pressure need to be cooled. A very low temperature for the compounds can be achieved using liquid N_2 and ethanol cooling bath.The mixing chamber is connected to the cryostat using a Cu tubing and a sample holder containing DCPhAc. One end of the Cu tubing was connected to the mixing chamber and other end to sample holder which was connected to the cryostat, so that the sample/inert gas mixture carries along with it the vapours of the solid sample. The flow rate while deposition was controlled using a needle valve (Model: EVN 116, Pfeiffer Vacuum) and was typically maintained~3 mmol/hr connected to an effusive nozzle. The vacuum shroud was mounted with all parts attached to it in the sample container of FTIR spectrometer. Each time an observation had to made, the expander was rotated within vacuum shroud to switch from matrix deposition mode to observation mode. Fig. 2.6 shows sample introduction assembly.

4. FTIR

A Bruker-Tensor 27 FTIR Spectrophotometer was used to obtain information about matrix isolated species (Fig. 2.7). A more detailed information is obtained due to its very high resolution of 0.5cm^{-1}. The spectra were recorded in region of 4000 to 400 cm^{-1} and a total of 8 scans were coadded to obtain good signal-to-noise ratio. First a spectra was recorded at 12K when the matrix was frozen. Then the temperature of the matrix was raised depending on the matrix gas used for the experiment, 27 K and 32 K for N_2 and Ar matrices respectively. The process of raising the temperature and allowing them to diffuse, remove

unstable sites, allow complex formation followed by cooling is called annealing. The temperature was again set back to 12 K to obtain an annealed spectra.

The home built matrix isolation setup is shown in Fig. 2.8.

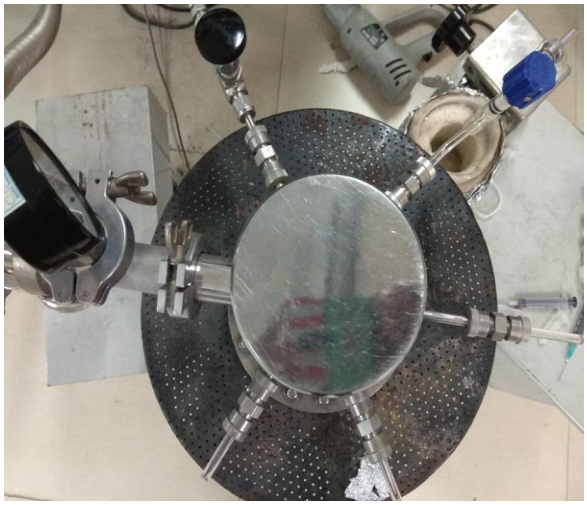

Mixing Chamber (Top view)

Mixing Chamber (side view)

Pressure gauge to monitor deposition

Needle Valve

Figure 2.6 Sample introduction assembly

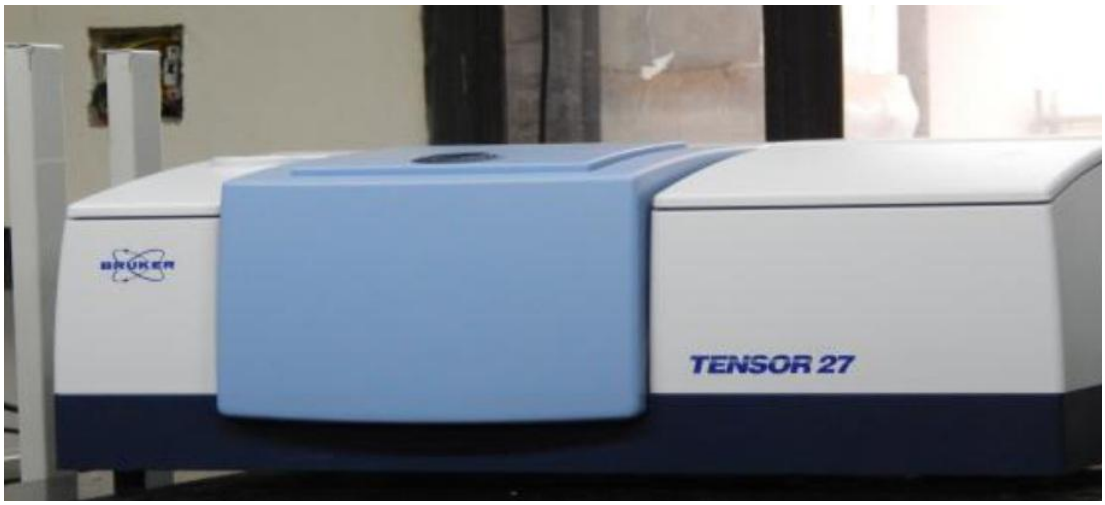

Figure 2.7 FTIR spectrometer

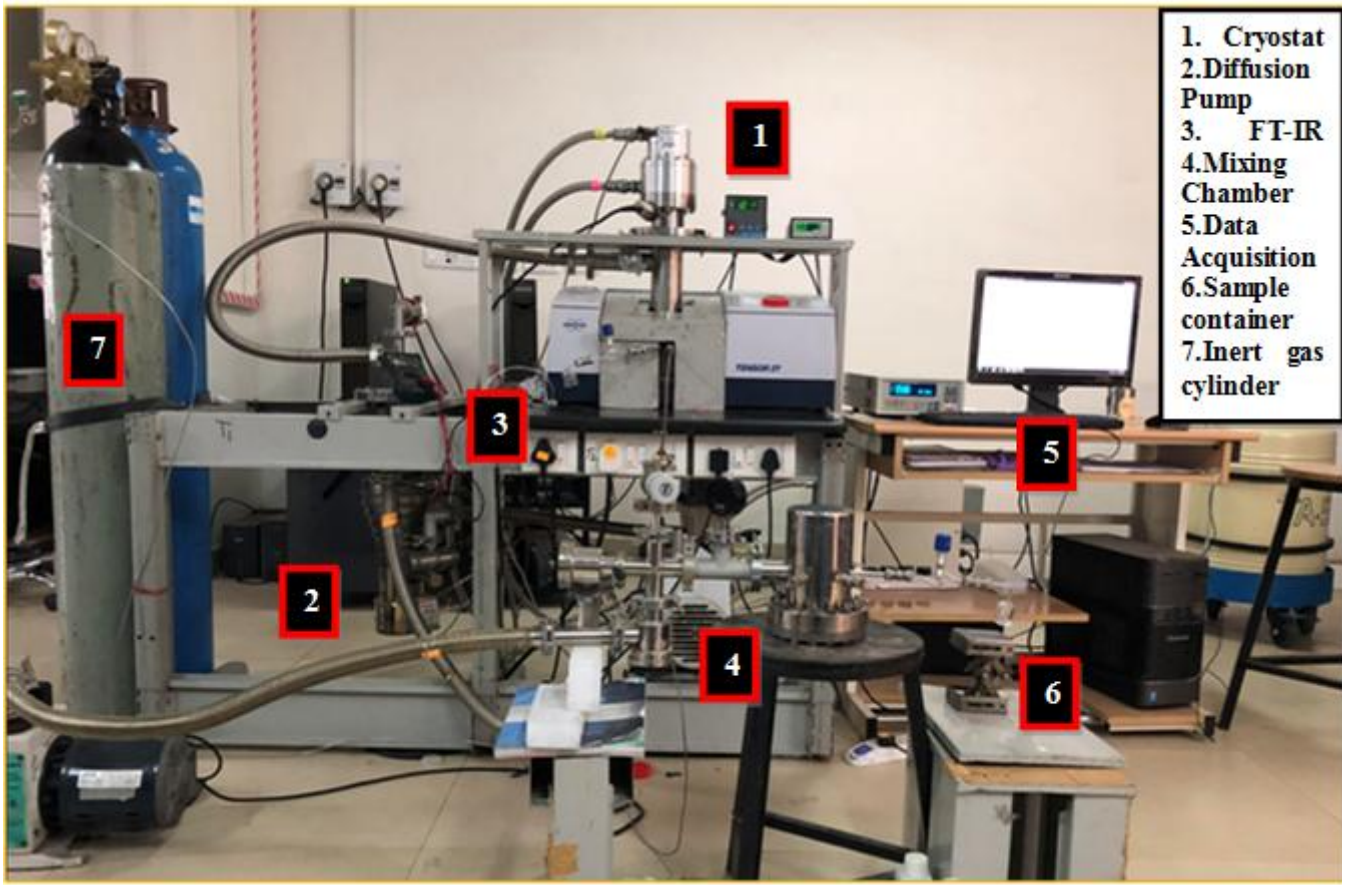

Figure 2.8 Home built Matrix Isolation setup at IISER

2.5 Synthesis of target 2,6-DCPhAc molecule

Synthesis of 1,3-dichloro-2-iodobenzene

1,3-dichloro-2-iodobenze was synthesized by the diazotization procedure. [34] Commercially available 2,6-dichloroaniline (2.00 g, 12.34 mmol,Himedia, purity 98.5%) was used as the precursor compound for *in situ* generation of diazonium salt, by slowly adding $NaNO_2$ (18.51 mmol) in cold water in presence of conc. HCl (37.03 mmol) while maintaining the temperature between0-5 ^oC. Then KI (49.36 mmol) dissolved in H_2O was added slowly to the above reaction mixture while stirring it continuously. White coloured precipitates were obtained. The reaction was continuously monitored by TLC and was completed in 2 hrs. Product was purified by column chromatography on silica gel and eluted with hexane to give 2.39 g (8.76 mmol, 71 %).Characterization was done using ^1H and ^{13}C NMR. The synthesis scheme of 2,6-DCPhAc is shown in Fig. 2.9.

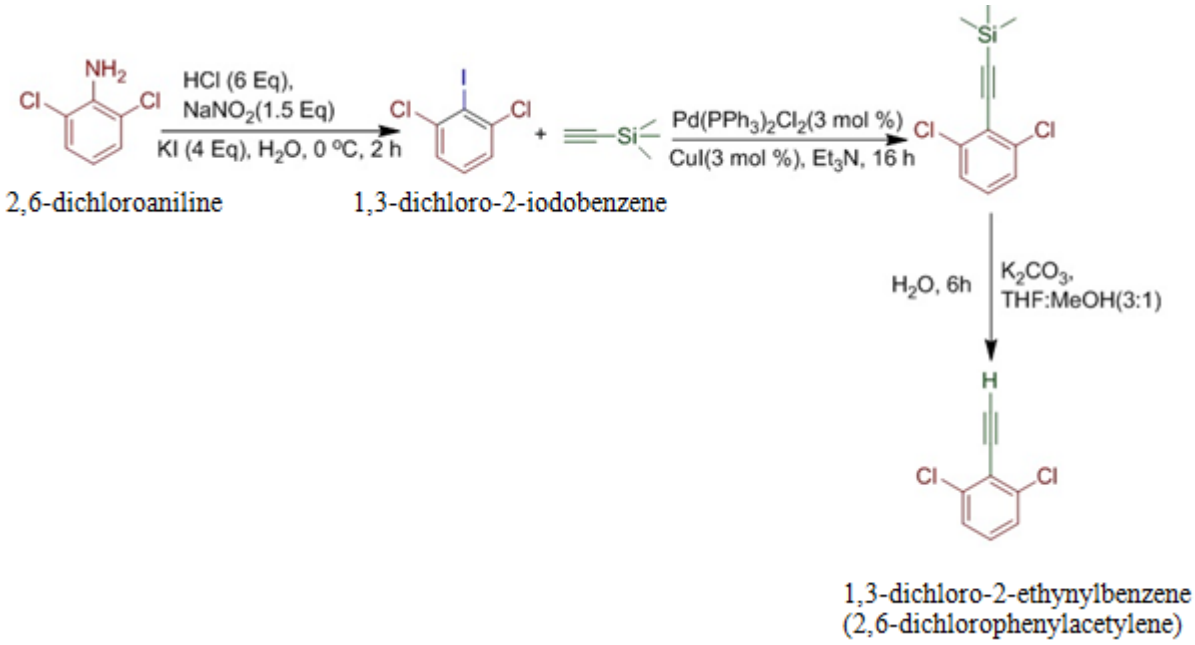

Figure 2.9 Scheme to synthesize 2,6-DCPhAc

Synthesis of 1,3-dichloro-2-ethynylbenzene [2,6-dichlorophenylacetylene (2,6-DCPhAc)]

2,6-DCPhAc was synthesized by Sonogashira coupling reaction.[35] The reaction was carried out under dry and inert conditions. First Et_3N (20 ml) was added to the three-necked

round bottom flask was purged with N_2 gas while stirring it continuously. The previously synthesized compound, 1,3-dichloro-2-iodobenze (1.00g, 3.66 mmol) and CuI (0.11 mmol) were added to the reaction mixture. The reaction was stirred for 15 min under the inert conditions and trimethylsilylacetate (7.33 mmol) was added. The reaction mixture was maintained at 65 ºC and reaction was completed in 16 hrs. The reaction mixture was filtered on ceilite and washed with hexane. The crude product was obtained by evaporating the solvent under reduced pressure which was later purified on SiO_2 column using hexane as the eluent to give 0.85 g (3.50 mmol, 95%) pure product. Characterization was done using ^1H and ^{13}C NMR.

The target molecule was obtained by deprotecting the trimethylsilyl group. For deprotection, first the product obtained was dissolved in THF (3 ml) and MeOH (1 ml). Anhydrous K_2CO_3(9 mg in 0.3 ml H_2O) was added to the reaction mixture and stirred for 6 hrs at room temperature. Reaction completion was confirmed by TLC. The product formed was extracted using hexane and H_2O. The organic layer was dried in rotavap. The crude was purified on SiO_2 column using hexane as eluent to obtain 0.23 g (1.33 mmol, 82 %) analytically pure white solid product. The characterization was done using ^1H and ^{13}C NMR. (Fig 2.10 and Fig. 2.11)

^1H NMR (400 MHz, $CDCl_3$): δ 3.69 (s, 1H), 7.19-7.23 (t, J = 8.1 Hz, 1H), 7.33-7.36 (d, J = 8.0 Hz, 2H), ^{13}C NMR (100 MHz, $CDCl_3$): 77.37, 88.01, 122.29, 127.71, 129.87, 137.95

2.6 Computational Methods

2.6.1 Geometry Optimization and Frequency Calculation

The first step to study amolecule computationally is performing a geometry optimization to locate minimum energy structures on potential energy surface referred to as stationary points (SP). All structures were optimized using Gaussian-09 package[36] on a Fujitsu Workstation. First, the individual molecules involved in complex formation were optimized. These optimized geometries of the individual molecules together were used as an input to optimize various possible structures which can lead to complex formation**.** Geometry optimizations usually locate the stationary point which is closest to initial guess geometry. Hence, various initial guess geometries were given as an input to obtain structures of various possible complexes. The successful optimization is the one which is able to locate the SP. where the

forces are zero. The convergence criteria defined by Gaussian 09 suite of programmes to locate a SP is when the forces, the root mean square of forces, the calculated displacements and the root mean square of displacement falls below a certain threshold values. The computations were performed using MP2 and DFT (M06-2X) methods, and aug-cc-pVDZ basis sets.

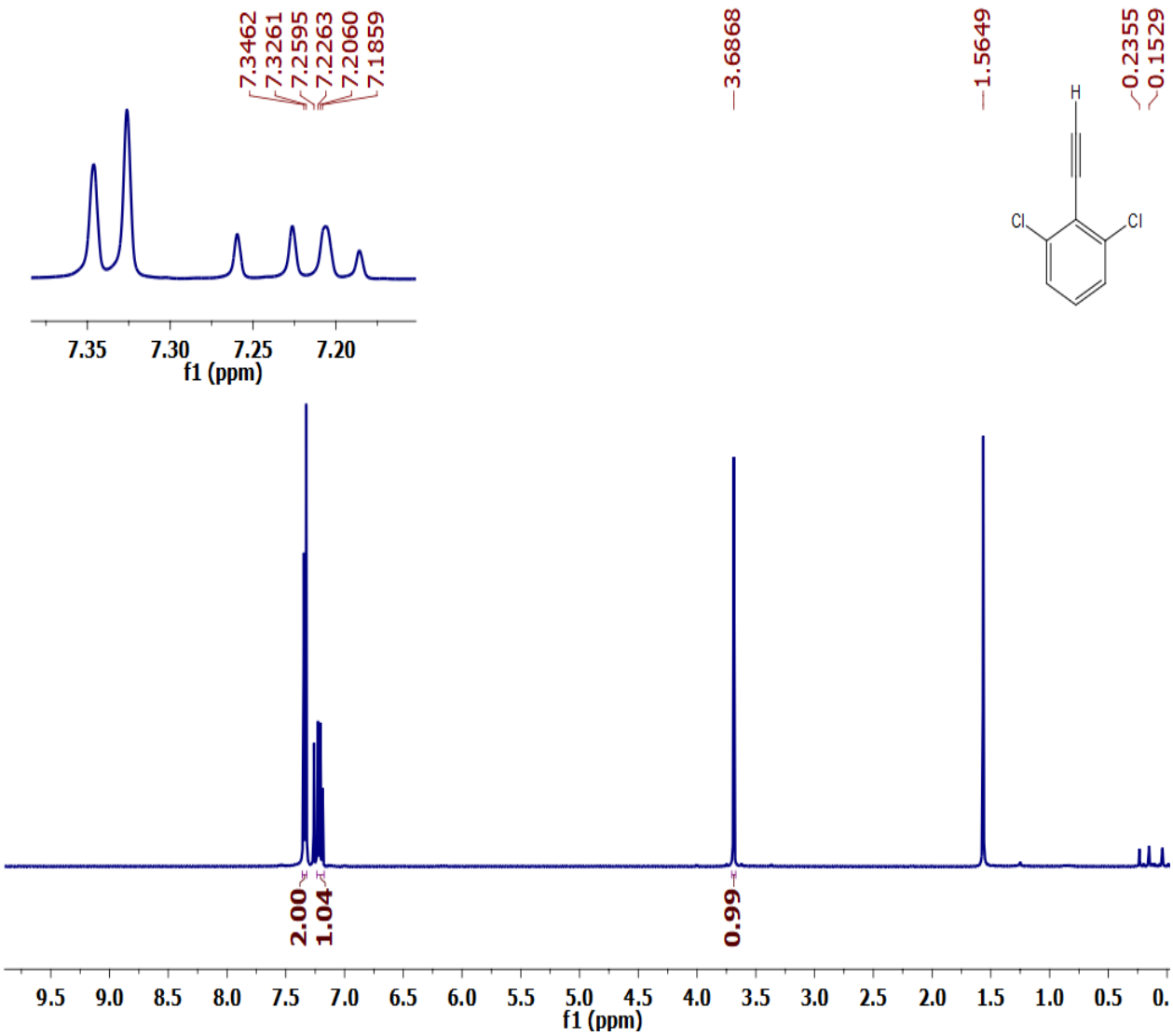

Figure 2.10 ^{1}H NMR (400 MHz, $CDCl_3$) spectrum of 2,6-DCPhAc

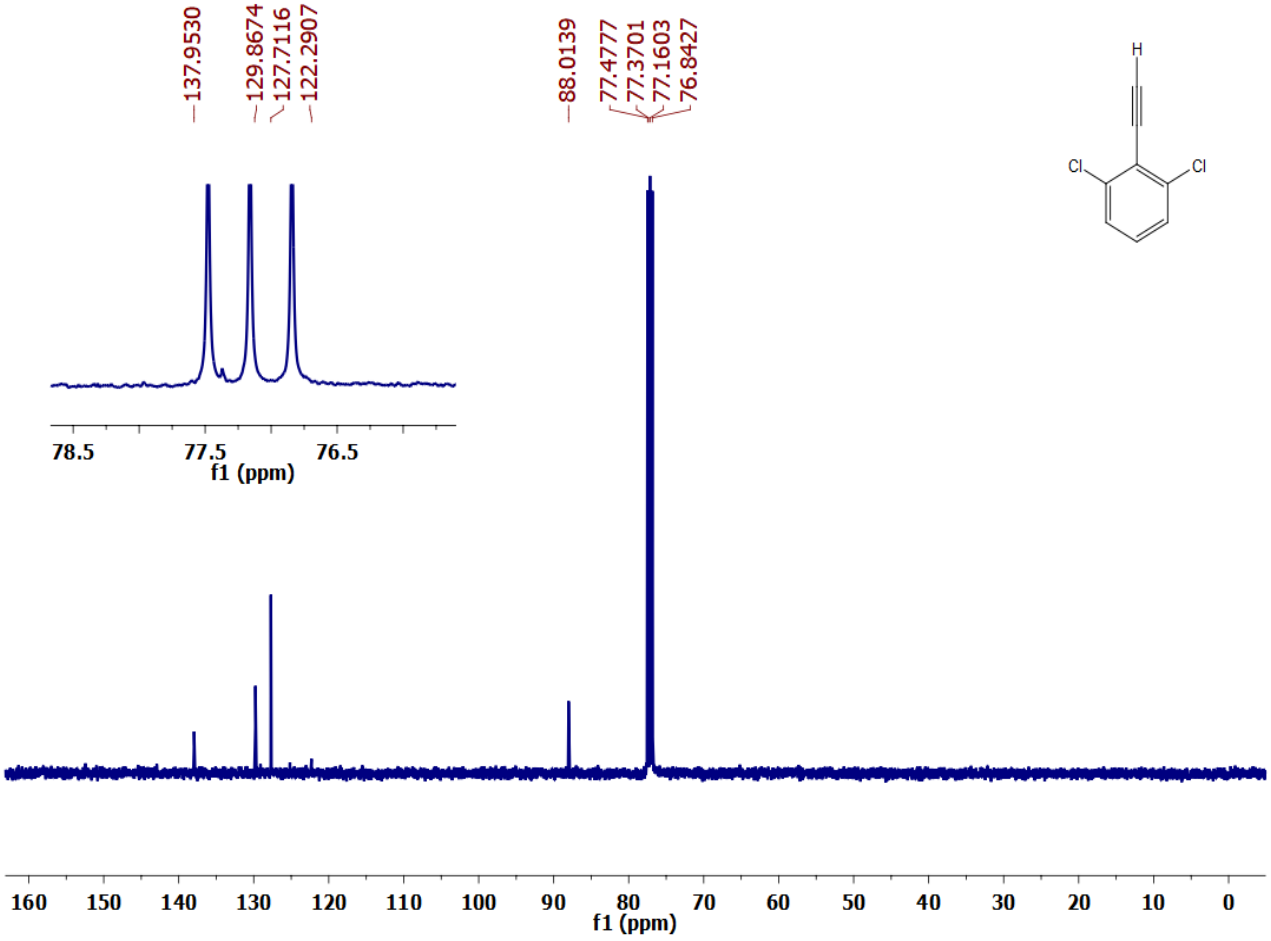

Figure 2.11 ^{13}CNMR (400 MHz, $CDCl_3$) spectrum of 2,6-DCPhAc

Single point calculations were also performed at MP2/aug-cc-pVTZ, MP2/aug-cc-pVQZ, CCSD/aug-cc-pVDZ and CCSD(T)/aug-cc-pVDZ using the optimized geometries at MP2/aug-cc-pVDZ level. As suggested by Vincent *et al.*[37] the optimization and frequency calculations done using opt=tight and int=ultrafine keywords at M06-2X level of theory in Gaussian 09.

A successful optimization is able to locate a SP, but it might not be the intended minima. A geometry optimization does not contain any information regarding nature of the SP. It is possible that the located SP might be a global minimum, a local minimum or a

saddle point. To distinguish between a minima and a saddle point, harmonic frequency calculations were performed on optimized structures at same level of theory.

For a minima, all the computed frequencies are positive. Structures having imaginary frequencies are considered as saddle points. The frequency calculations were also used to corroborate the experimental results. For comparison, the computed frequencies were scaled. The scaling factors were determined by bringing the computed values in agreement with experimental values. The computed spectra were plotted using the scaled frequencies using a spectrum synthesis program, Synspec.[38] The computed spectra was obtained using a Lorentzian lineshape and a full width at half maximum (FWHM) of 1.0 cm^{-1}.

2.6.2. Interaction Energy

A super-molecular approach was employed to calculate interaction energies denoted by E. The interaction energy between two atoms or molecules A and B is calculated as the energy difference between the product complex AB and its monomers A and B and given by.

$E = E_{AB} – (E_A+E_B)$

where, E_A, E_B and E_{AB} are energies of monomers A and B and the complex formed between A and B respectively.

A negative interaction energy indicates that the complex formed is stable relative to its monomers. It needs be corrected to account for zero point energy (ZPE) and basis set superposition error (BSSE). Both the corrections were included separately, otherwise it can result in overcorrected stabilization energies.[39,40]

The ZPE corrected interaction energies, E_{ZPE}, were calculated as follows:

$E_{ZPE} = E + ZPE$

The wavefunction of a monomer is expanded in lesser basis functions than the wavefunction of the complex, resulting in stabilization of a complex more than the separate components. This inconsistency is attributed to basis set superposition error and can be eliminated if the monomer A is allowed to use additional basis function from monomer B and vice-versa. Typically counterpoise (CP) method, proposed by Boys and Bernadi is employed for removing BSSE.[41] To calculate energy of monomer A, $E_A(AB)$ by employing CP method, the basisfunctions on monomer B on all its atomic centers are used, while neglecting their electrons and nuclear charges. These basis functions are called ghost

function and atoms of B are called the ghost atoms. Similarly the energy of monomer B, $E_B(AB)$ is calculated. The BSSE corrected interaction energies are calculated as follows:

$E_{BSSE} = E_{AB}(AB) – E_A(AB)- E_B(AB)$

Where $E_A(AB)$, $E_B(AB)$ are energies of monomer A and B respectively, using basis set of AB and $E_{AB}(AB)$ is the energy of complex AB using basis set of AB. MP2 complete basis set limit interaction energies ($\Delta E_{MP2/CBS}$) were also calculated using a two point extrapolation method by Helgaker*et al.*[42]given by:

$$\Delta E_{MP2/CBS} = \frac{4^3 \times \Delta E(pVQZ) - 3^3 \times \Delta E(pVTZ)}{4^3 - 3^3}$$

The interaction energies at CCSD(T) complete basis set limits ($\Delta E_{CSSD(T)/CBS}$) were also calculates as follows:

$$\Delta E_{CCSD(T)/CBS} = \Delta E_{MP2/CBS} + \Delta E_{CCSD(T)/aug-cc-pVDZ} + \Delta E_{MP2/aug-cc-pVDZ}$$

2.6.3 Atoms-in-Molecules (AIM) Analysis

The presence of hydrogen bonding can be determined using Bader's theory of 'atoms-in-molecules' which uses a criteria based on charge density.[43]Since any interaction between the two nuclei affects the charge density ρ(r), AIM theory is based on topological analysis of ρ(r)to confirm the presence of various interactions. In this thesis, AIM analysis was performed to unravel weak non-covalent interactions such as X-H···π, hydrogen bonds, halogen bonds, *etc*. The points in space where the first derivatives of ρ(r) vanishes, i.e. ∇ ρ(r)=0 are referred to as critical points (CPs). Whether the point is a maxima, a minimum or a saddle point can be determined by the sign of the second derivatives. For an arbitrary choice of coordinate axes, a total of nine second derivatives are possible. These are given by a 3x3 symmetric matrix, generally referred to as a Hessian matrix of the charge density. It is diagonalized to obtain eigenvalues; λ_1, λ_2 and $\lambda_3$also known as principal axis of curvature. The sum of eigenvalues is known as Laplacian ($\nabla^2\rho$) and it plays an important role in the characterization of chemical bonding. The rank of a CP, denoted by ω, is the number of non zero eigenvalues and signature, denoted by σ is the algebric sum of the signs of eigenvalues. A CP is describes as (ω,σ) and it can takes four possible values; (3, -3), (3, -1), (3, +1) and (3, +3). A (3, -1) CP exists when there is a chemical bond between any two nuclei suggesting a bond formation, a (3, +1) CP is found in interior of a ring and is known as a ring critical

point (RCP), a (3, +3) CP is called a cage critical point (CCP) and a (3, -3) CP corresponds to a minima. The number of critical points which can coexist in a system with a finite number of nuclei, are governed by Poincare-Hopf relationship given by:

$n - b + r - c = 1$

where, n is the number of nuclei, b is the number of bond critical points, r is number of RCPs and c is number of CCPs.

The AIM2000[44] software was used to analyze the properties of atoms in molecules. The wavefunctions generated for the optimized geometries using Gaussian 09 software were given as input to AIM2000.In order to confirm hydrogen bonding, the charge density $\rho(r)$ value were examined to be within the range 0.002-0.034 a.u. and $\nabla^2\rho(r)$ in the range 0.024-0.139a.u. at the bond critical point as suggested by Koch and Poplier.[45] Besides this, the sign of $\nabla^2\rho(r)$ is indicative of the types of interaction BCP to be either closed shell interactions as in the case of ionic, hydrogen bonded and van der Waals complexes or a shared-shell interaction existing in case of covalent bonding. A positive sign of $\nabla^2\rho(r)$ indicates a close shell interaction which means that there is the depletion of electronic charge between a pair of atoms. A negative sign is indicative of a shared shell type interaction suggesting that there is a concentration of electronic charge between the pair of atoms involved in bonding.

Furthermore, a method proposed by Espinosa *et al.*[46]was employed to determine the interaction energy (ΔE_{HB}) due to each contact by using local kinetic density, $G(r_{CP})$ and local potential energy density $V(r_{CP})$.

2.6.4 Localised Molecular Orbital Energy Decomposition Analysis (LMO-EDA)

Intermolecular interactions are the key to discern the formation of various systems of interest, and hence it becomes important to quantify these chemical effects. EDA serves as a novel approach to partition intermolecular interaction energy into various energy components such as electrostatic, charge transfer, polarization *etc.* There are many different approaches to decompose the interaction energy which are a result of various definitions of interaction energy that comes from different types of interactions under consideration. The level of theory limits the scheme to be implemented for energy decomposition. EDA can be implemented to analyze covalent as well as intermolecular interactions. According to Su and Li, Hartree-Fock (HF) methods, the total interaction energy can be decomposed into electrostatic, exchange, repulsion, and polarization terms given by:

$$\Delta E_{int} = \Delta E_{elec} + \Delta E_{ex} + \Delta E_{rep} + \Delta E_{pol}$$

Dispersion energy can be calculated using second order Moller-Plesset theory (MP2) and coupled cluster methods like CCSD and CCSD(T).

$$\Delta E_{int} = \Delta E_{elec} + \Delta E_{ex} + \Delta E_{rep} + \Delta E_{dis} + \Delta E_{pol}$$

The individual contributing terms obtained by decomposing the interaction energy are defined as follows:

1. Electrostatic (ΔE_{elec}): the localised interaction between the occupied molecular orbitals, not involving any mixing of the orbitals.
2. Polarization (ΔE_{pol}): the interaction involves mixing between the occupied and the vacant molecular orbitals of the molecules.
3. Exchange (ΔE_{ex}): the interaction between occupied molecular orbitals cause electron exchange and delocalisation between molecules.
4. Repulsion (ΔE_{rep}): the interaction arises as a result of pauli's exclusion principle and is repulsive in nature.
5. Dispersion (ΔE_{dis}): the interaction which arises due to instantaneous and induced dipole interactions.

In this thesis, LMO-EDA (Localized Molecular Orbital EDA) was used to partition the interaction energy of hydrogen bonded complexes of 2,6-DCPhAc with H_2O. EDA uses the existing programs in GAMESS to perform self-consistent field (SCF) calculations on basis of single determination HF (restricted closed shell HF, restricted open shell HF and unrestrtricted open shell HF) and their density functional theory analogues. LMO-EDA was used to understand the nature of interactions.

2.6.5 Natural Bond Orbital (NBO) Analysis

NBO analysis provides the electronic density distribution on atoms and bonds.It is a helpful tool in understanding the delocalization of the electron density, hyperconjugation effects and most importantly both intramolecular and intermolecular bonding interactions. It was developed by Weinhold and co-workers, and used to understand and quantify the hydrogen bonding interactions occurring when there occurs an overlap between donor and acceptor orbitals. [47] A stable donor-acceptor interaction takes place when there is delocalization of electron density between the occupied (bond or lone pair)NBO orbitals and unoccupied (antibonding or Rydberg) orbitals. The basis of NBO analysis is transforming a

given wavefunction into a localized form, i.e. to the one center (‘lone pair’) and two-center (‘bond’) which draws a Lewis structure picture for a chemist. The NBO program performs the analysis of a many-electron molecular wavefunctions in terms of localized electron-pair bonding units. It is achieved by transforming the input atomic orbitals into natural bond orbitals (NBOs) via natural atomic orbitals (NAOs) and natural hybrid orbitals (NHOs).

NBO analysis was performed on the molecule using pop=nbo keyword through the Gaussian 09 package, at the MP2/aug-cc-pVDZlevel, to elucidate the intramolecular hydrogen bonding. It gives the second order perturbation energies E to determine the extent of interaction between electron donor and acceptors, which depends on the overlap F(i,j) between the donor and the acceptor orbitals and is inversely proportional to the energy difference between the donor-acceptor orbitals [E(j)-E(i)]. Hence, the greater the value of E, the more is the donating tendency of an electron donor to an electron acceptor. Various vibrational shifts observed in a spectrum can be understood using NBO analysis. For instance, a red shift is observed when there is a transfer of electron density from a bonding orbital to an antibonding orbital, which leads to weakening of a bond leading to a red shift.

Chapter 3

Results and Discussion

3.1 Experimental Details

All experiments were performed using $N_2$and Ar were (Sigma & Gases, 99.999%) as the matrix gases. 2,6-DCPhAc was synthesized (procedure described in Ch-2), H_2O (millQ, 16-18 Ω) and D_2O (Merck, 99.9%) were used without any further purification. The precursor compounds were subjected to several freeze-pump-thaw cycles before mixing the sample and matrix gas in the mixing chamber. Gas mixtures with the appropriate matrix to sample ratios were prepared using standard manometric procedures.

2,6-DCPhAc and H_2O were first deposited separately and the infrared spectra was recorded. To study complex formation, both precursors were codeposited. Some experiments were also performed using D_2O to study the isotopic effect.2,6-DCPhAc was maintained at appropriate temperatures to obtain vapour pressures which when mixed with the matrix gas, yielded spectra of matrix isolated sample. Since, 2,6-DCPhAc is a solid, it was kept close to the deposition window and the matrix gas premixed with H_2O was passed over the solid. This helped in sweeping of vapours of 2,6-DCPhAc to the deposition window, together with matrix gas. As 2,6-DCPhAc was deposited in the matrix using a transpiration method, we could not calculate the exact sample to matrix ratio for 2,6-DCPhAc. We varied the concentration of 2,6-DCPhAc in the matrix by maintaining it at different temperatures. To avoid dimer or multimer formation, it was ensured that the concentration of 2,6-DCPhAc was not high. The sample to matrix ratio of H_2O was varied from 0.5:1000 to 2.8:1000. The sample and matrix gas mixture was deposited on to the cold KBr window at a deposition rate of ~3 mmol/hr using a single jet effusive nozzle. After deposition, the matrix temperature was raised to 27 K for N_2 matrix (32 K for Ar matrix), maintained at this temperature for 30 minutes and then recooled to 12 K. This process was to encourage diffusion of the precursors and aid complex formation, which was signalled by new features that appear after annealing.

3.2 Computational Details

Ab initio calculations were performed at MP2 and M06-2X levels of theory and 6-311++G(d,p) and aug-cc-pVDZ basis sets. Monomers were optimized individually and the

optimized geometries were then used for optimizing the geometry of hydrogen bonded complexes. The structures of the complexes obtained at MP2/aug-cc-pVDZ are shown in Fig. 3.1 with geometrical parameters listed in Table 3.1. Harmonic frequency calculations were done at the same level of theory as geometry optimization to ensure that all frequencies were positive and to assign the experimentally observed features. Frequency calculations indicated the absence of any imaginary frequency, which confirmed that all the optimized structures were indeed minima on the potential surface. The interaction energies were computed using supermolecule approach and were corrected for zero point energy (ZPE) and basis set superposition errors (BSSE) separately[48] at various levels of theory are shown in Table 3.2.

The computed frequencies were scaled to corroborate the experimentally observed frequencies in the following way. The strongest feature observed in the experiments in a given spectral region was correlated with the strongest computed features for the monomers. The scaling factors were determined by bringing the computed values of the submolecule in agreement with its experimental values and this scaling factor was then used to scale the computed frequencies of the complexes. In matrix isolation experiments, there are various matrix effects which are responsible for perturbing various frequency modes differently. Hence, mode-by-mode scaling is employed, where the above mentioned scaling procedure is followed to determine the scaling factor for each spectral region separately. The computed spectra were plotted using these scaled frequencies employing spectrum synthesis program, Synspec.[38] The computed spectral features were plotted with Lorentzian lineshape and a full width at half maximum (FWHM) of 1.0 cm^{-1}.

The AIM2000 software was used to analyze the properties of atoms-in-molecules by the theory of R. Bader.[43] The wavefunctions generated for the optimized geometries using Gaussian 09 software were provided as inputs. Presence of hydrogen bonding contacts were confirmed by locating the appropriate bond critical points (BCP). the The charge density $\rho(r)$ and $\nabla^2\rho(r)$ values were calculated at BCP's. LMO-EDA was used to partition the interaction energy of hydrogen bonded complexes into electrostatic, polarization, exchange, repulsion and dispersion components and to understand the nature of interaction. NBO analysis was done to determine the electronic density distribution on atoms and bonds and to understand and quantify the hydrogen bonding interactions, manifested by the overlap between donor and acceptor orbitals.

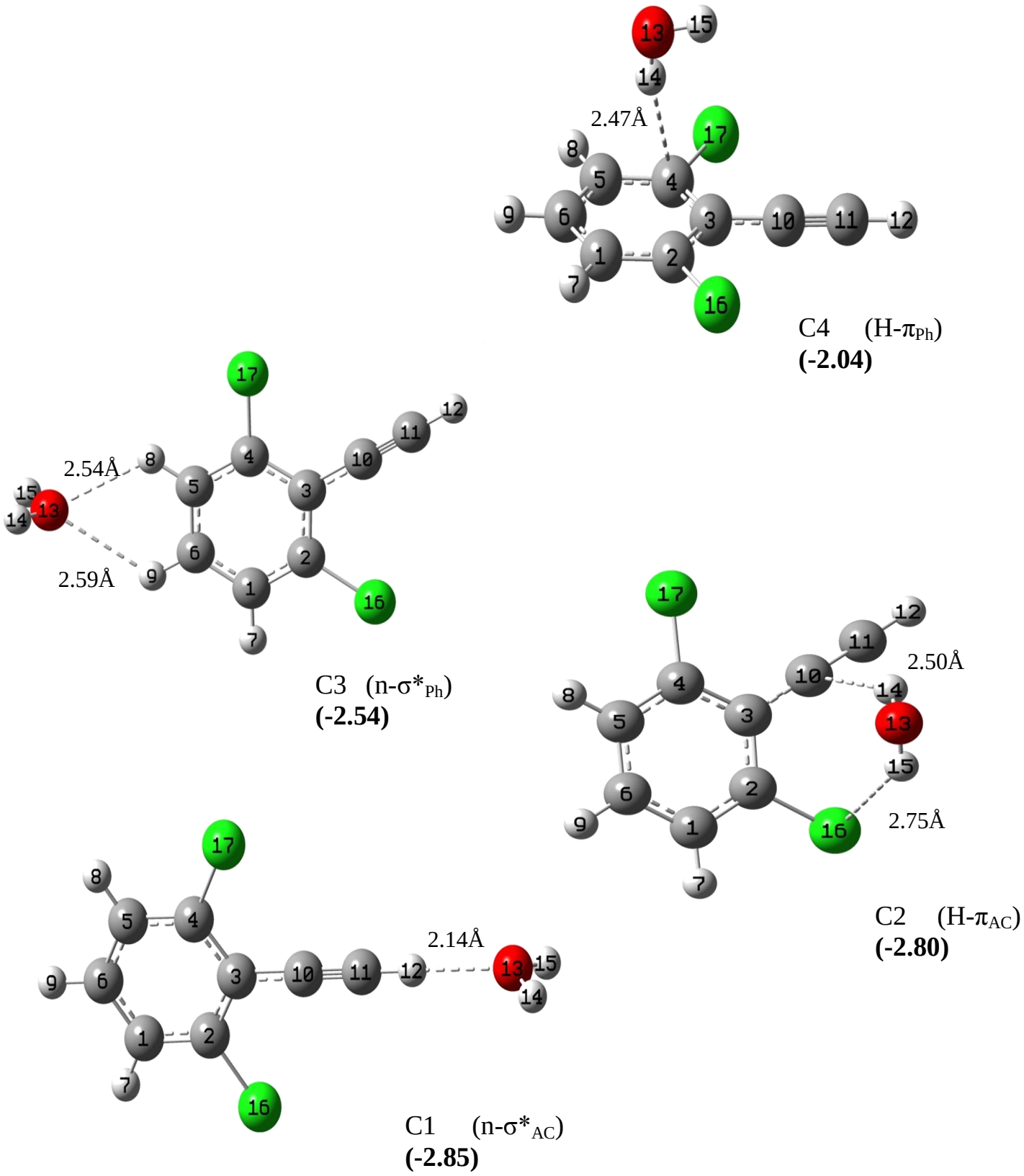

Figure 3.1 Optimized geometries of 2,6-DCPhAc-H_2O complexes at MP2/aug-cc-pVDZ level of theory. BSSE corrected interaction energy (kcal/mol) at MP2/aug-cc-pVDZ level of theory are given in parenthesis. (See text for details.)

Table 3.1 Important geometrical parameters, bond length (Å), bond angles (º), dihedral angles(º), for 2,6DCPhAc-H_2O complexes computed at the MP2/aug-cc-pVDZ level. Labelling of atoms is shown in Fig. 3.1.

C1		C2		C3		C4	
O_{13}-H_{12}	2.14	Cl_{16}-H_{15}	2.75	O_{13}-H_8	2.54	H_{14}-C_4	2.47
H_{14}-O_{13}-H_{12}	124.3	H_{14}-C_{10}	2.50	O_{13}-H_9	2.59	O_{13}-H_{14}-C_4	166.6
H_{14}-O_{13}-H_{12}-C_{11}	-76.6	H_{14}-C_{11}	2.74	H_{15}-O_{13}-H_8	120.6	H_{14}-C_4-Cl_{17}	110.8
		O_{13}-H_{15}-Cl_{16}	140.3	H_{14}-O_{13}-H_9	124.2	H_{15}-O_{13}-H_{14}-C_4	-13.5
		O_{13}-H_{14}-C_{10}	138.8	C_8-O_{13}-H_9	57.8	H_{15}-O_{13}-H_{14}-C_5	-169.3
		O_{13}-H_{14}-C_{11}	157.8	H_{14}-O_{13}-H_9-C_6	-107.6		
		H_{15}-Cl_{16}-C_2	82.1	H_{15}-O_{13}-H_8-C_5	-113.9		
		H_{14}-C_{10}-C_3	91.7				
		O_{13}-H_{14}-C_{11}-H_{12}	-115.5				
		O_{13}-H_{14}-C_{10}-C_{11}	-148.9				
		O_{13}-H_{15}-Cl_{16}-C_2	-36.9				
		H_{15}-O_{13}-H_{14}-C_{10}	44.2				
		H_{15}-O_{13}-H_{14}-C_{11}	6.10				

Table 3.2 Interaction energies for the various 2,6-DCPhAc-H_2O complexes at different levels of theory. Interactions energies have been given as Raw/ZPE corrected/BSSE energies (kcal/mol). Where only one entry is given, they are uncorrected energies. (See text for details).

Complex	M06-2X		MP2			CCSD(T)	
	6-311++G(d,p)	aug-cc-pVDZ	6-311++G(d,p)	aug-cc-pVDZ	CBS	aug-cc-pVDZ	CBS
C1	-3.98/-2.75/-3.29	-3.39/-2.24/-2.93	-4.04/-2.62/-2.43	-4.00/-2.90/-2.85	-3.03	-4.02	-3.05
C2	-4.57/-3.48/-3.60	-4.24/-3.00/-3.77	-4.91/-3.89/-1.94	-4.85/-3.75/-2.80	-3.63	-4.77	-3.56
C3	-3.88/-2.70/-3.21	-3.18/-2.18/-2.82	-3.71/-2.92/-2.28	-3.56/-2.66/-2.54	-2.74	-3.64	-2.82
C4	-	-	-5.08/-3.94/-1.60	-4.70/-3.87/-2.04	-2.69	-4.43	-2.42

3.3 Results

3.3.1 Experimental Results

Hydrogen bonded complexes of 2,6-DCPhAc with H_2O were studied both experimentally and computationally. The experiments were performed in both N_2 and Ar matrices. Since the spectra were sharper in N_2matrix, only the N_2 matrix spectra are shown.

Fig. 3.2 shows the ≡C-H stretching region (3350-3200 cm^{-1}) of 2,6-DCPhAc. The monomer feature due to ≡C-H stretch appears as a Fermi diad at 3308.7 and 3317.0 cm^{-1}. Fermi resonance occurs as a result of the coupling between the acetylenic ≡C-H stretch acetylenic C≡C stretching and two quanta of acetylenic C-H out of plane bending vibrational modes.[49] On codeposition of 2,6-DCPhAc and H_2O, a very strong product feature was observed at 3232.9 cm^{-1}. In Fig. 3.3, the 810-770 cm^{-1} region corresponds to acetylenic ≡C-H bending of 2,6-DCPhAc. The features were observed at 800.2 cm^{-1}which was due to the phenyl ring deformation and at 780.2 cm^{-1}due to the phenyl –CH out-of-plane motion coupled with ≡C-H out-of-plane bend. A new product feature was observed at 781.8 cm^{-1} (Fig. 3.3). These regions are highly sensitive towards any type of weak interaction and act as markers for the presence of hydrogen bonding interactions.

The product features were not present when precursors alone were deposited, and hence can be assigned to the complex. Furthermore, these product features were also observed at very low concentration of both 2,6-DCPhAc and H_2O and are therefore assigned to a 1:1 complexes. H_2O is an unavoidable impurity in matrix isolation experiments, so very weak features of product bands were also observed at 12 K. The product features however shows an increase in intensity on increasing the concentration of either precursor, which reaffirms that the new features observed were due to the formation of hydrogen bonded complexes between 2,6-DCPhAc and H_2O.

To study the isotopic effects, experiments were also performed with D_2O instead of H_2O. The O-D antisymmetric stretch of D_2O is observed at 2766.1 cm^{-1}. When 2,6-DCPhAc and D_2O were codeposited, the features due to HOD masked the features corresponding to complexes making the assignments in this region somewhat difficult.

3.3.2 Computational Results

The monomers, 2,6-DCPhAc and H_2O are both multifunctional molecules, having a both proton acceptor and proton donor sites. The monomer 2,6-DCPhAc can act as a proton acceptor through chlorine, acetylenic π cloud, phenyl π clouds and as proton donor through acetylenic hydrogen and phenyl hydrogens. Similarly, H_2O is also amphiprotic molecule having both proton accepting and donating sites. Therefore one can expect to observe multiple isomers of 2,6-DCPhAc-H_2O adduct.

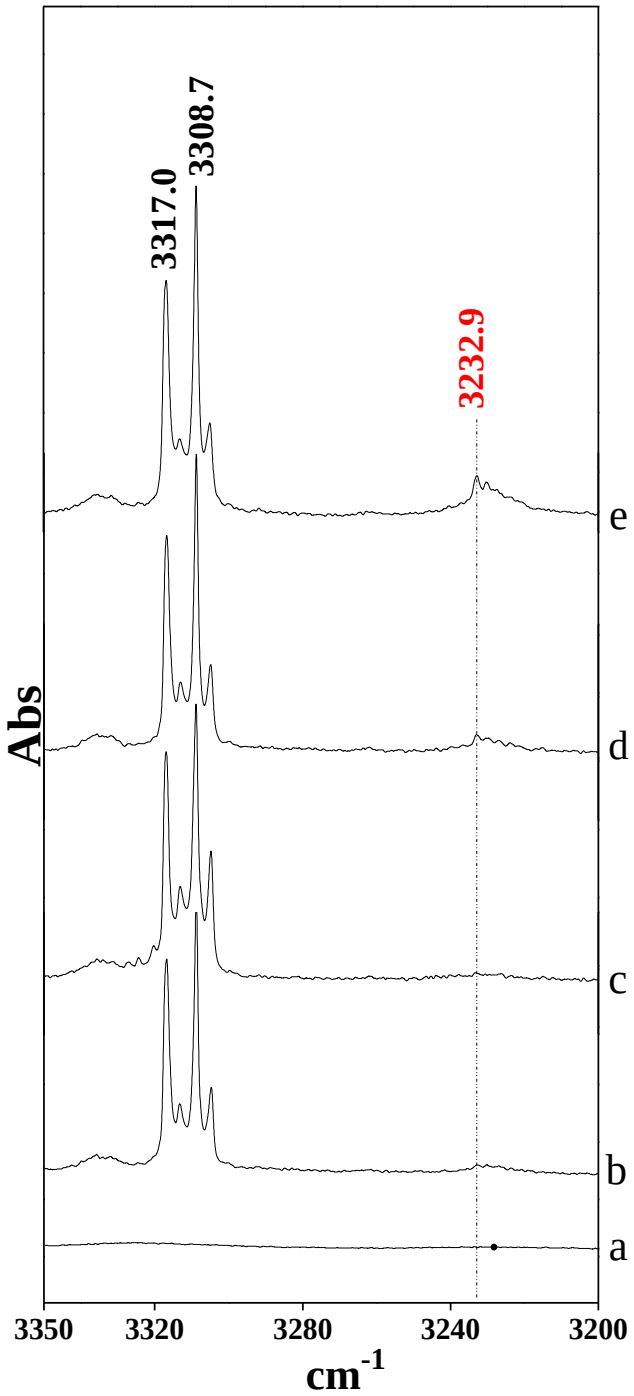

Figure 3.2 Spectra of 2,6-DCPhAc-H_2O complexes in N_2 matrix in ≡CH stretching region of 2,6-DCPhAc (3350 – 3200 cm^{-1}) (a) H_2O: N_2 (0.5:1000) (b) 2,6-DCPhAc: N_2 (x:1000) (c) 2,6-DCPhAc: H_2O:N_2 (x:0.5:1000) (as deposited) (d) 2,6-DCPhAc: H_2O:N_2 (x:0.5:1000) (e) 2,6-DCPhAc: H_2O:N_2 (x:2.8:1000). All spectra, except that shown in trace (c), were recorded after annealing the matrix at 27 K. Spectrum in trace 'c' was recorded after depositing the matrix (before annealing).

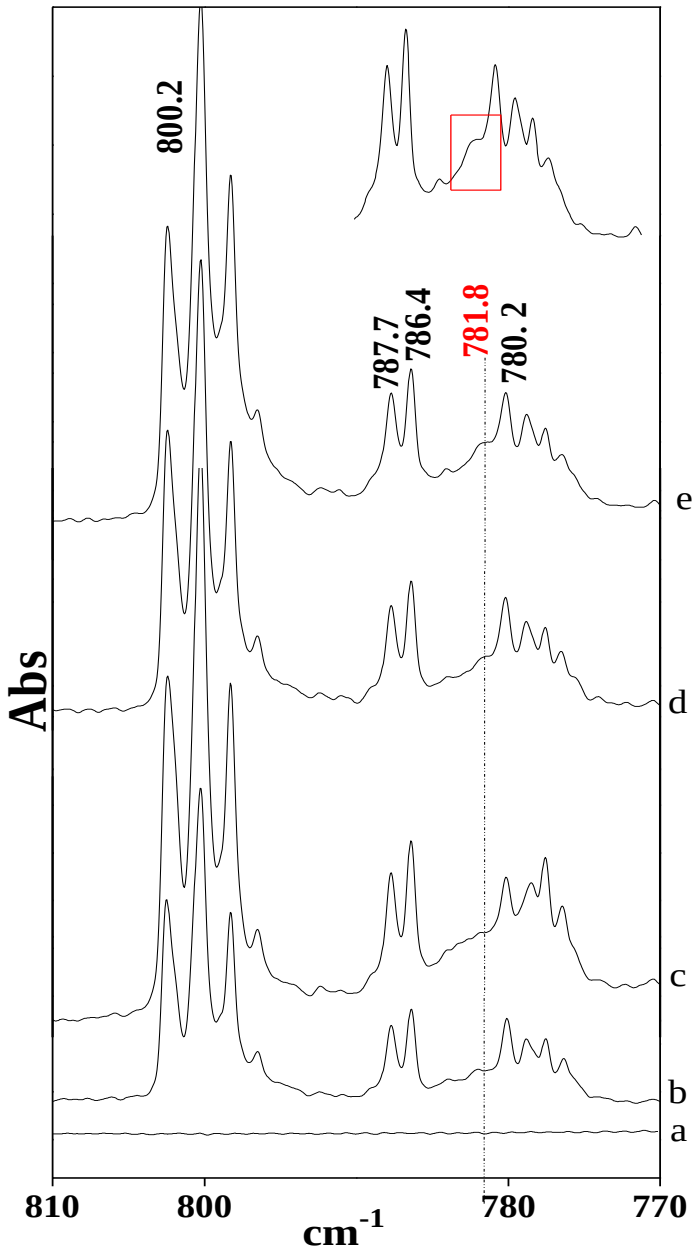

Figure 3.3 Spectra of 2,6-DCPhAc-H_2O complexes in N_2 matrix in ≡CH bending region of 2,6-DCPhAc (810-770 cm^{-1}) (a) H_2O: N_2 (0.5:1000) (b) 2,6-DCPhAc: N_2 (x:1000) (c) 2,6-DCPhAc: H_2O:N_2 (x:0.5:1000) (as deposited) (d) 2,6-DCPhAc: H_2O:N_2 (x:0.5:1000) (e) 2,6-DCPhAc: H_2O:N_2 (x:2.8:1000). All spectra, except that shown in trace (c), were recorded after annealing the matrix at 27 K. Spectrum in trace 'c' was recorded after depositing the matrix (before annealing).

While at MP2/6-311++G(d,p) and MP2/aug-cc-pVDZ levels, we obtained four optimized hydrogen bonded structures at M062X/6-311++G(d,p) and M062x/aug-cc-pVDZ levels, we obtained only three optimized structures. Fig. 3.1 shows optimized geometries of hydrogen bonded structures of 2,6-DCPhAc-H2O complexes at MP2/aug-cc-pVDZ level of theory.

Complex 1 (n-σ^*_{AC}) - The acetylenic hydrogen acts as a proton donor to H_2O.
Complex 2 (H-π_{AC}) - H_2O acts as a proton donor to both, acetylenic π cloud and Cl of 2,6-DCPhAc.
Complex 3 (n-σ^*_{Ph}) - H_2O acts as a proton acceptor form phenyl hydrogens.
Complex 4 (H-π_{Ph}) - H_2O acts as a proton donor to phenyl π cloud.

At M062X/6-311++G(d,p) and M062X /aug-cc-pVDZ levels, complex 2 is most stable, followed by complex 1 and 3 for raw, ZPE corrected and BSSE corrected energies. Complex 4 was not observed at this level. A similar trend was observed at MP2/6-311++G(d,p) and MP2/aug-cc-pVDZ levels, complex 2 being most stable, followed by complex 1, 3 and 4 for raw, ZPE corrected energies. The same trend was observed at complete basis set (CBS) limits also. However when one considers the the BSSE corrected values, the energy ordering flips making complex 1 more stable than complex 2, followed by complex 3,4. The results have been presented in Table 3.2. However, it should be noted that the energy difference between complexes 1 and 2 are much smaller than the energy difference between the corresponding complexes in PhAc-H_2O. As shown in Fig. 3.1, the shortest hydrogen bond is computed to be present in complex 1,where the acetylenic hydrogen donated proton to oxygen on H2O which is not in same plane as 2,6-DCPhAc. In complex 2, there are two interactions which have a bond distance greater than that of complex 1. The H_2O is out of plane such that one of the its hydrogen interacts with acetylenic π cloud and the other interacts with Cl of 2,6-DCPhAc.

Since the experimental results matches best with the results obtained computationally at MP2/aug-cc-pVDZ level of theory, the results have been reported at the same level of theory and it is used for further analysis.

3.4 Discussions

Vibrational Assignments

The vibrational assignments have been summarized in Table 3.3. The computed and experimental spectra are shown in Fig. 3.4 and Fig. 3.5.

3.4.1 Vibrational features of 2,6-DCPhAc submolecule

≡C-H stretching region

The new product feature is observed at 3232.9 cm^{-1} in the ≡C-H stretching region of 2,6-DCPhAc. The computed spectra for all the four complexes along with the experimental spectra are shown in Fig. 3.4. The product feature shows a experimental red shift of 84.1 cm^{-1}. The complexes 1, 2 and 4 show a computed red shift of 70.1 cm^{-1}, 4.8 cm^{-1} and 1.9 cm^{-1} respectively. Only complex 3 show a computed blue shift of 0.9 cm^{-1}. Table 3.3 shows that the computed shift for complex 1 is in agreement with experimentally observed shift. The observation of the similar n-σ* complex for PhAc-H_2O system in ≡C-H stretching region was reported by Karir *et al.*, which also amounted to such a large red shift in frequency.[19] Hence, the 3232.9 cm^{-1} feature can be unambiguously assigned to complex 1. These shifts are also in agreement with the magnitude of the reported complexes of PhAc- methanol and PhAc-ether complexes.[50] Hence, the n-σ* complex is observed in the matrix.[51] The calculated shifts for complexes 2, 3 and 4 are very small, these features if at all present, probably overlap with features observed for ≡C-H stretching mode of 2,6-DCPhAc. It is difficult therefore to assign with any certainty, features for any of these complexes, if indeed they were formed in the matrix.

≡C-H bending and phenyl -C-H bending

A monomer feature was observed at 780.2 cm^{-1}which corresponds to phenyl –CH out-of-plane bend (Fig. 3.5). There was also another feature observed at 625.2 cm^{-1} corresponding to ≡C-H in plane bend. In the phenyl –CH bending region, a product feature is observed at 781.8 cm^{-1}. On comparing it with the computed frequencies for all the four complexes, it is hard to assign this feature with respect to a particular bending mode. Given that complex 1 is lower in energy than other complexes, and also the fact that it is present in the matrix, the 781.8 cm^{-1} feature can be tentatively assigned to complex 1.

3.4.2 Vibrational features of H_2O submolecule

The product vibrational features were not observed in H_2O stretching or bending region unambiguously as these were masked by other H_2O dimer and multimers features.

Table 3.3 Experimental, scaled computed vibrational wavenumbers (cm^{-1}) and vibrational mode assignments for2,6-DCPhAc and its complexes with H_2O and D_2O. Computations are done at the MP2/aug-cc-pVDZ level of theory.

Experimental (cm^{-1})		Scaled Computed Wavenumbers (cm^{-1})					Mode Assignment
		Monomer	Complex 1	Complex 2	Complex 3	Complex 4	
2,6DCPhAc	1:1 Complex		2,6-DCPhAc-H_2O				
3317.0	3232.9 **(-84.1)**	3317.0	3247.0 **(-70.1)**	3312.2 (-4.8)	3317.9 (0.9)	3315.1 (-1.9)	≡C-H stretch
780.2	781.8	761.8	758.4 [a]	762.3	785.2	768.0	Phenyl –CH op bend[b]
625.2	-	625.2	784.8 (159.5)	628.2 (3.0)	621.5 (-3.7)	633.4 (8.1)	≡C-H ip[b] bend
H_2O							
3727.9	-	3753.0	3748.7 (-4.3)	3714.3 (-38.7)	3743.7 (-9.3)	3724.8 (-28.2)	OH antisym. stretch
3635.5	-	3625.0	3622.7 (-2.3)	3603.5 (-21.5)	3617.2 (-7.8)	3603.8 (-21.1)	OH sym stretch
1597.7	-	1597.7	1599.2 (1.6)	1604.3 (6.6)	1603.5 (5.9)	1589.7 (-8.0)	OH bend
D_2O			2,6-DCPhAc-D_2O				
2766.1	-	2749.1	2746.2 (-2.9)	2719.3 (-29.8)	2742.2 (-6.9)	2727.4 (-21.7)	OD antisym stretch
2655.6	-	2596.6	2612.1 (15.5)	2599.0 (2.4)	2608.4 (11.8)	2599.0 (2.4)	OD sym stretch
1178.9	-	1169.1	1170.7 (1.6)	1173.6 (4.5)	1173.1 (4.0)	1163.0 (-6.1)	OD bend

Numbers in parenthesis are $\Delta\nu = \nu$(complex)- ν(monomer)
Scaling Factors : 0.95312(3800-2000 cm^{-1}) , 0.98482 (2000-1000 cm^{-1}), 1.00016 (1000-400 cm^{-1})
[a]Strong coupling between ≡C-H op bend of 2,6-DCPhAc and phenyl –CH op bend of 2,6-DCPhAc.
[b]op: out-of-plane, ip: in-plane

3.5 AIMS Analysis

The atoms-in-molecules theory of Bader,[43] based on topological analysis of charged density was used to confirm the presence of various hydrogen bonding contacts in complexes using the wavefunction generated at MP2/aug-cc-pVDZ level of theory. The bond critical points (3,-1) and ring critical points (3,+1) were located for the optimized structures. Various

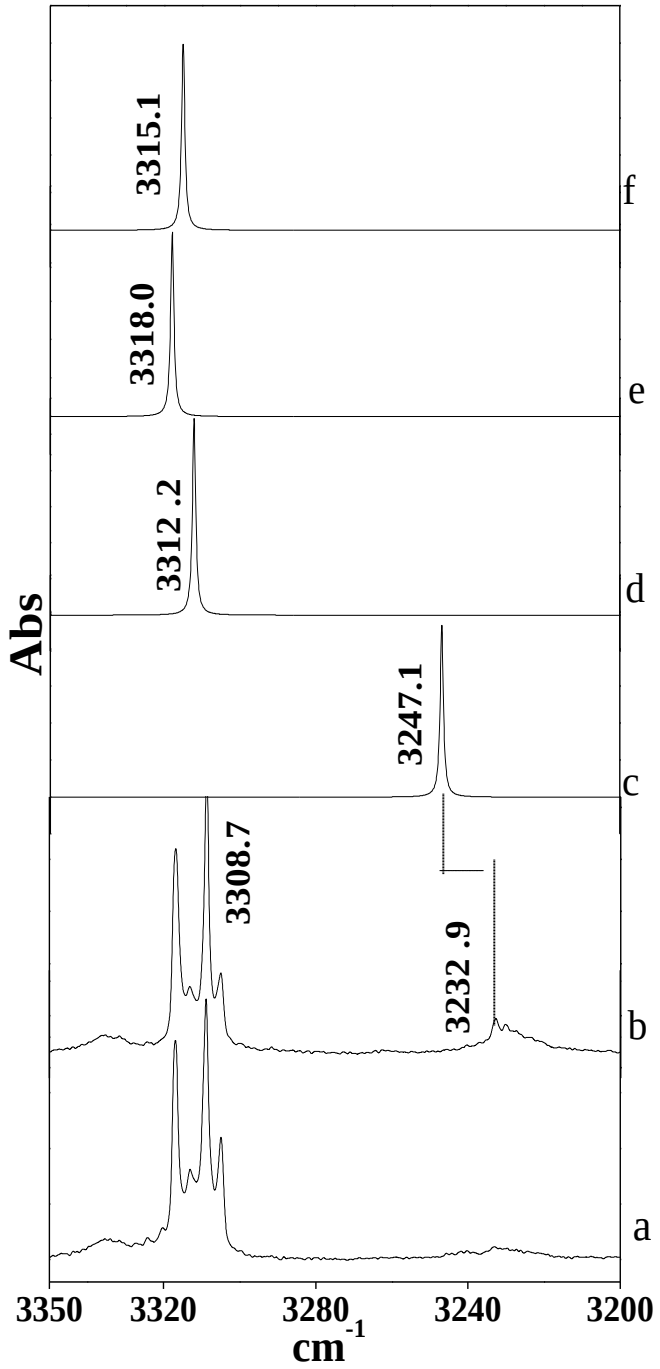

Figure 3.4 Experimental and computed infrared spectrum of 2,6-DCPhAc-H_2O complexes in N_2 matrix in ≡CH stretching region of 2,6-DCPhAc (3350 – 3200 cm^{-1}) (a) 2,6-DCPhAc: H_2O: N_2 (x:2.8:1000) (as deposited), (b) 2,6-DCPhAc: H_2O:N_2 (x:2.8:1000) (annealed at 27 K), (c) Computed spectra of complex 1, (d) Computed spectra of complex 2, (e) Computed spectra of complex 3, (f) Computed spectra of complex 4.

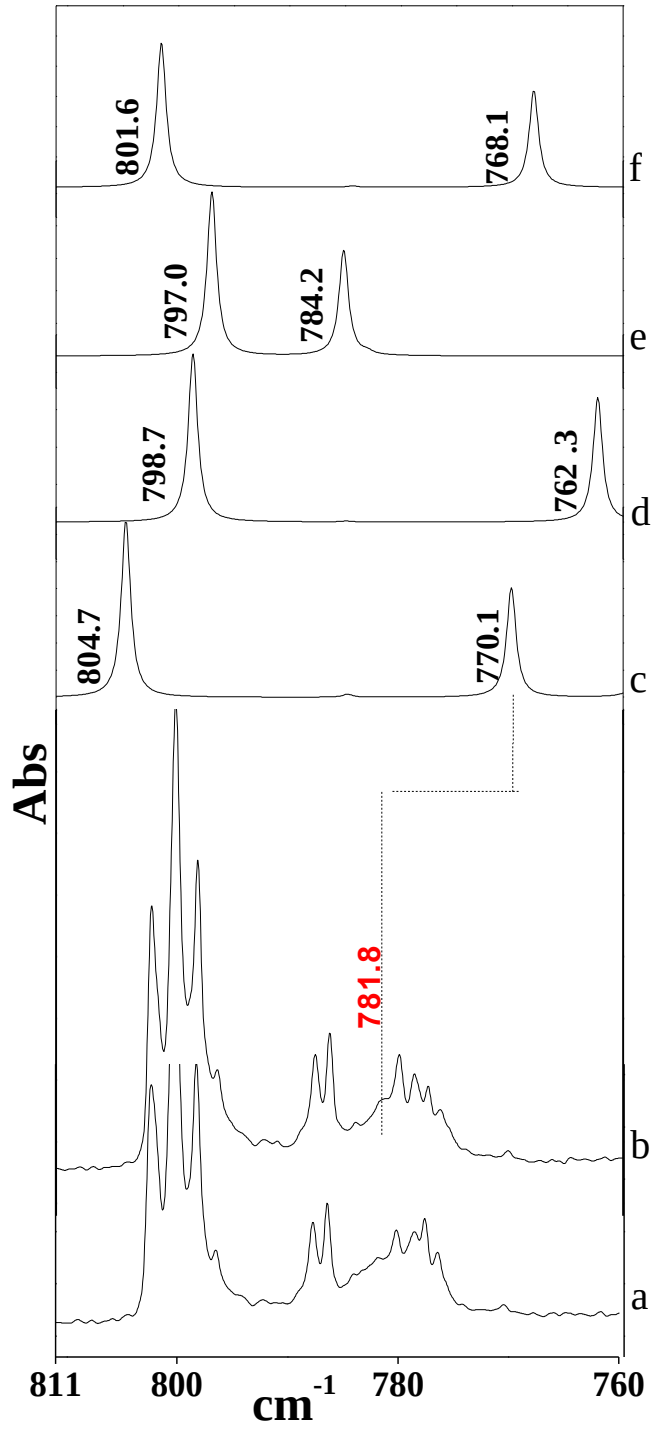

Figure 3.5 Experimental and computed infrared spectrum of 2,6-DCPhAc-H_2O complexes in N_2 matrix in ≡CH bending region of 2,6-DCPhAc (811-760 cm^{-1}) (a) 2,6-DCPhAc: H_2O: N_2 (x:2.8:1000) (as deposited), (b) 2,6-DCPhAc: H_2O:N_2 (x:2.8:1000) (annealed at 27 K), (c) Computed spectra of complex 1, (d) Computed spectra of complex 2, (e) Computed spectra of complex 3, (f) Computed spectra of complex 4.

topological parameters such as charge density $\rho(r_c)$, eigenvalues of the Hessian matrix (λ_1,λ_2,λ_3) and the Laplacian ($\nabla^2\rho$) of charge density were computed at the bond critical pointsand are listed in Table 3.4.The $\rho(r_c)$ and $\nabla^2\rho$ values lie within the range of 0.002-0.034 a.u. and 0.024-0.139 a.u. respectively, which is the range for existence of a hydrogen bonding interaction as suggested by Koch and Poplier.[45] A positive value of $\nabla^2\rho$ indicated a closed shell type interaction. Various bond critical points located in the structures are shown in Fig. 3.6. As is evident from Table 3.4, the strongest interaction was observed in complex 1 (C-H···O) having largest values for both $\rho(r_c)$ and $\nabla^2\rho$. In complex 2, two bond critical points were observed, one involving a stronger (O-H···π) interaction and another secondary (O-H···Cl) interaction. ΔE_{HB} indicates the strength of individual hydrogen bond contact in complexes as calculated by Espinosa's method. We observe that the sum of O-H···π and C-Cl···O in H-π_{AC} complex (complex 2) is less than the single C-H···O contact in n-σ^*_{AC} complex (complex 1), indicating that the latter is indeed the global minimum. This is in contrast to PhAc-H_2O system, where H-π_{AC} becomes the global minimum due to presence of weaker secondary C-H···O interaction.

Table 3.4 Summary of AIM calculations (MP2/aug-cc-pVDZ level) for the 2,6-DCPhAc-H_2O complexes. All quantities are expressed in a.u. See text for definition of each of the quantities.

Complex	$\rho(r_c)$	$\nabla^2\rho(rc)$	λ_1	λ_2	λ_3	$\lvert\lambda_1/\lambda_3\rvert$	(λ_1/λ_2)-1	ΔE_{HB}	Total E
C1	0.0155	0.0529	-0.0179	-0.0168	0.0876	0.2043	0.0655	-3.13	-3.13
C2 bcp1	0.0098	0.0293	-0.0082	-0.0056	0.0431	0.1902	0.4643	-1.58	-2.86
bcp2	0.0082	0.0257	-0.0067	-0.0060	0.0384	0.1745	0.1167	-1.28	
C3 bcp1	0.0085	0.0308	-0.0082	-0.0071	0.0461	0.1779	0.1549	-1.45	-2.71
bcp2	0.0075	0.0283	-0.0071	-0.0059	0.0413	0.1719	0.2034	-1.26	
C4	0.0106	0.0306	-0.0086	-0.0039	0.0431	0.1995	1.2051	-1.73	-1.73

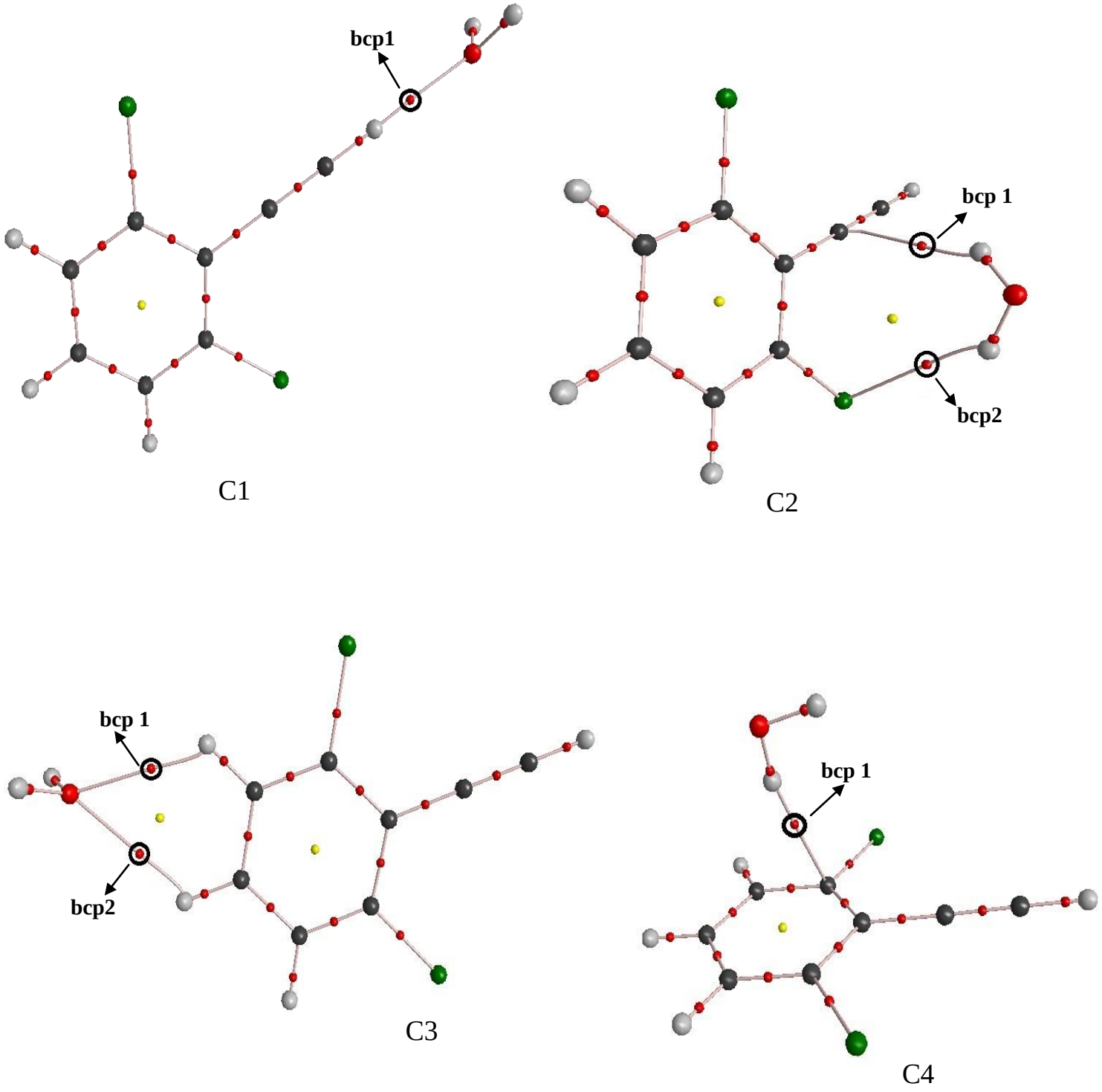

Figure 3.6 AIM analysis on the optimized geometries of the 2,6-DCPhAc-H_2O complexes, obtained at MP2/aug-cc-pVDZ level of theory. Bond critical points (bcp) corresponding to the intermolecular interactions have been indicated.

3.6 NBO Analysis

The natural bond orbital analysis (NBO) analysis was performed on all the optimized structures of 2,6-DCPhAc and H_2O complexes. The results have been summarized in Table 3.5. The table lists the second order perturbation energies (E), donor and acceptor orbital energy difference [E(j)-E(i)] and the overlap between the donor and acceptor orbital [F(i,j)]. The strongest interaction is observed in complex 1, which involves donation of electron density from lone pair on oxygen of H_2O to antibonding orbital of acetylenic C-H of 2,6-DCPhAc. Complex 2 involves two interactions. The stronger one involves donation of electron density from acetylenic π orbital to antibonding orbital of O-H of H_2O and there was also a presence of a hydrogen weak interaction between Cl on 2,6-DCPhAc and O-H of H_2O. In complex 3 and 4, the interactions were relatively weaker as compared to what was observed in complexes 1 and 2.

Table 3.5 NBO analysis of 2,6-DCPhAc-H_2O complexes at MP2/aug-cc-pVDZ level of theory. The atom numbering indicated in the table is as shown in Fig. 3.1. E is the second order perturbation energy (kcal/mol), E(j)-E(i) is the donor-acceptor energy difference and F(i,j) is the overlap between the donor and acceptor orbitals.

Complex	Orbital Involved		E(kcal/mol)	E(j)-E(i) a.u.	F(i,j) a.u.	Electron occupancy in σ* orbital
	Donor	Acceptor				
C1	O_{13}(n)	C_{11}-H_{12}(σ*)	7.16	1.61	0.096	0.013
C2	C_{10}-C_{11}(π)	H_{14}-O_{13}(σ*)	1.27	1.17	0.035	0.002
	Cl_{16}(n)	H_{15}-O_{13}(σ*)	1.06	1.25	0.033	0.002
C3	O_{13}(n)	C_5-H_8(σ*)	0.96	1.27	0.031	0.011
	O_{13}(n)	C_6-H_9(σ*)	0.76	1.60	0.031	0.010
C4	C_4-C_5(π)	O_{13}-H_{14}(σ*)	1.30	1.11	0.037	0.003

3.7 Energy Decomposition Analysis

The energy decomposition analysis was done for all the complexes to determine the contribution of electrostatic, exchange- repulsion, polarization and dispersion energy towards the total interaction energy of the complex. The results have been summarized in Table 3.6. The LMO-EDA scheme was implemented through GAMESS.[52] It is clear from the table that complexes 1 and 3, which involves n-σ* interaction, the electrostatic component contributes

significantly along with small contributions from dispersion and polarization components. In case of complex 2 and 4, which involved both n-σ* and H-π interactions, both electrostatic as well as dispersion interactions contribute significantly, with a comparatively small contribution from polarization. All the four complexes show a significant electrostatic interaction contribution except for complex 4. The results are consistent with what was obtained for AIMS analysis.

Table 3.6 LMO-EDA analysis for the various 2,6-DCPhAc-H_2O complexes at the MP2/aug-cc-pVDZ.

.

Complex	E_{ES}	E_{ER}	E_{Pol}	E_{Disp}	E_{Total}	E_{ES}/E_{Total}	E_{Pol}/E_{Total}	E_{Disp}/E_{Total}
C1	-4.92	3.96	-1.32	-0.59	-2.87	1.71	0.46	0.21
C2	-4.15	5.44	-1.35	-2.79	-2.85	1.46	0.47	0.98
C3	-3.67	2.82	-0.72	-1.02	-2.59	1.42	0.28	0.39
C4	-1.89	4.42	-1.28	-3.33	-2.07	0.91	0.62	1.61

Chapter-4

Conclusions

The complexes of 2,6-DCPhAc with H_2O were studied using matrix isolation infrared spectroscopy and the results were corroborated using computations. The 2,6-DCPhAc-H_2O system was compared with a recent study of the PhAc-H_2O system. The quasi planar structure global minimum structure observed in PhAc-H_2O was shown to have dual interactions, involving a primary O-H···π interaction and a weaker secondary C-H···O interaction. The OH of the H_2O which is involved in O-H···π interaction remains in the plane of PhAc, while the other hydrogen was out of the plane. The secondary C-H···O interaction was thought to be playing an important role in deciding the global minimum structure. It was the only plausible explanation as of why the H-π complex in PhAc-H_2O system should be the more stable structure than n-σ* complex , which is contrary to what is indicated by the gas phase acidity values.[53] Karir *et al.,* while pointing out the importance of these weak secondary interactions says that their role is more than just '*supportive*'. These are the '*decision makers*' of the H-π vesus n-σ* comepetition which exists whenever there are multifunctional molecules involved.

With a view to deciphering the importance of the secondary interaction, the C-H···O interaction was suppressed by replacing the ortho hydrogens in PhAc with Cl, thereby removing the C-H···O interaction. This change led to two changes. One was a change in the geometry of 2,6-DCPhAc-H_2O in H-π_{AC} complex, which was now observed to be non-planar. Even though the H-π structure in this system, still had two interactions, an O-H···π and a O-H···Cl interactions, the O-H···Cl interaction was observed to be very weak. Second and more importantly, a decrease in the energy gap between the H-π_{AC} and n-σ_{AC}* complexes was also observed, with H-π_{AC} complex still being more stable than n-σ_{AC}* complex, though the difference was less than in PhAc-H_2O. The energy gap in 2,6-DCPhAc-H_2O system reduced from 1.17 kcal/mol in PhAc-H_2O system to 0.6 kcal/mol at CBS limits at MP2 level of theory. A similar trend was observed at CCSD(T)/CBS level, with gap decreasing from 1.14 kcal/mol to 0.5 kcal/mol. More interestingly, flipping was observed between the two structures for the BSSE corrected interaction energy at MP2/aug-cc-pVDZ level of theory.

The n-σ_{AC}* complex became more stable than the H-π_{AC} complex by 0.05 kcal/mol in 2,6-DCPhAc-H_2O systems whereas it was higher in energy by 0.7 kcal/mol in PhAc-H_2O system. It starts mimicking the Ac-H_2O system in which there was no secondary interaction involved and n-σ* was observed to be the global minima both experimentally and computationally. The comparison among Ac-H_2O, PhAc-H_2O and 2,6-DCPhAc-H_2O systems have been depicted in Fig. 4.1.[53] All these studies point to one significant conclusion, that the suppression of the C-H···O interaction, decreased the energy difference between the H-π_{AC} and n-σ_{AC}* structures, thereby highlighting the role of the C-H···O interaction in such non-covalently bonded structures.

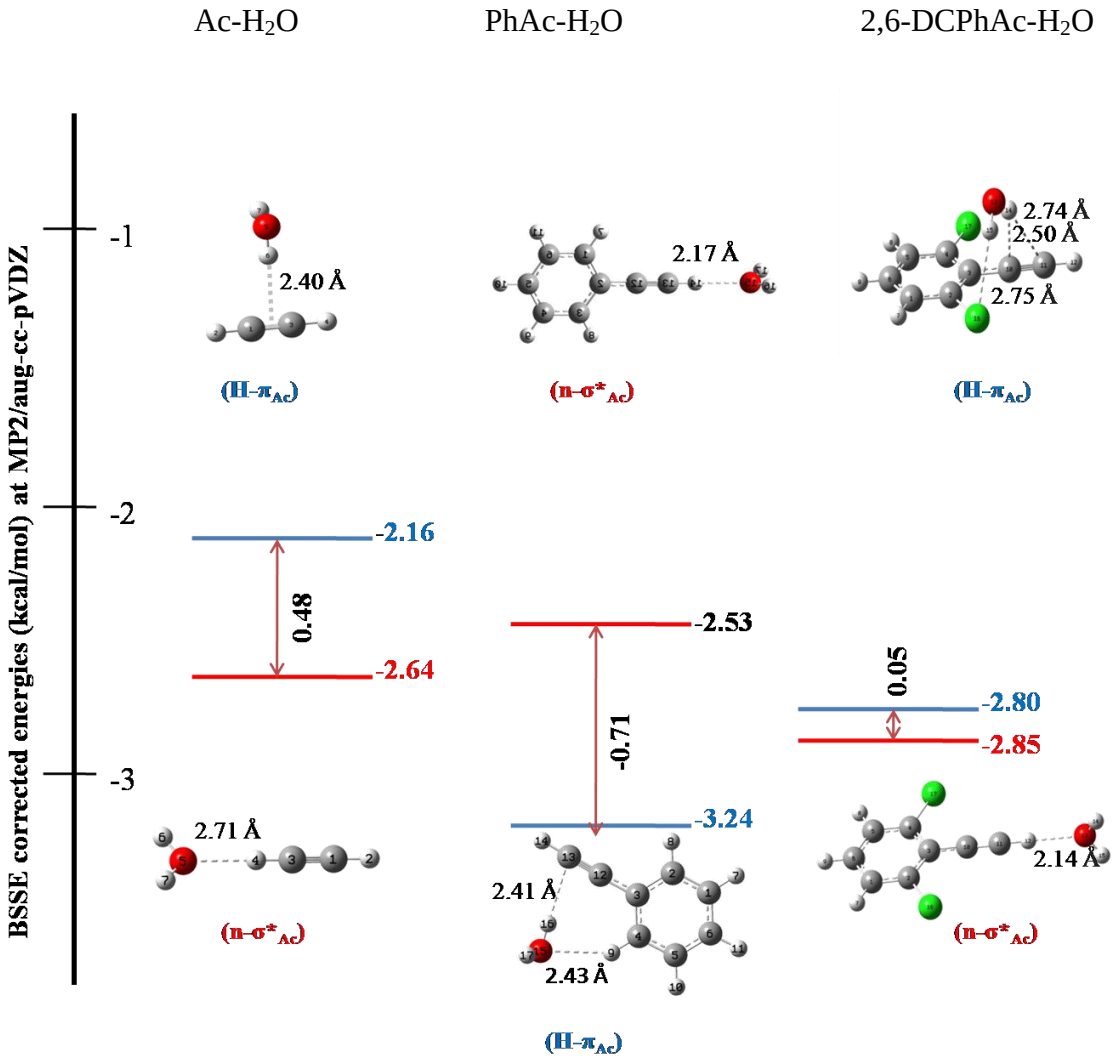

Figure 4.1 Energy differences between H-π and n-σ* structures in Ac-H_2O, PhAc-H_2O and 2,6-DCPhAc-H_2O systems.

This study provides an example of how secondary interactions can be tailored to influence the n-σ* and H-π competition in hydrogen bonded complexes. Hence, tailoring interactions can tilt the balance, favouring one structure over the other. This tilting of balance has been described in Fig. 4.2.

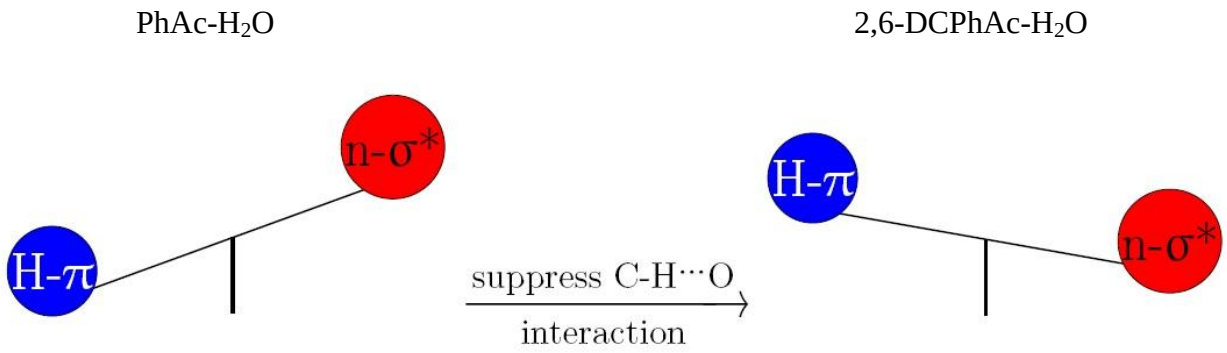

Figure 4.2 Tilting of balance on suppressing secondary interaction.

References

[1] Mali, K.S.; Pearce, N.; Feyter, D. S. Frontiers of Supramolecular Chemistry at Solid Surfaces. *Chem. Soc. Rev.* **2017**, *46*, 2520-2542.

[2] Hobza, P.; Müller-Dethlefs, K., Non-covalent Interactions: Theory and Experiment, Royal society of chemistry, 2009.

[3] Dethlefs, K.; Hobza, P. Non-covalent Interactions: A Challenge for Experiment and Theory. *Chem. Rev.***2000**, *100*, 143−167.

[4] Banerjee, P.; Chakraborty, T.Weak Hydrogen Bonds: Insights from Vibrational Spectroscopic Studies. *Int. Rev. Phys. Chem.* **2018**, *37*, 83-123.

[5] Del Bene, J.E.; Elguero, J.; Alkorta, I. Complexes of CO_2 with the Azoles :Tetral Bonds, Hydrogen Bonds and Other Secondary Interactions. *Molecules.* **2018,** *23***,** 906-926.

[6] Desiraju G.R. C–H···O and Other Weak Hydrogen Bonds: From Crystal Engineering to Virtual Screening. *Chem. Commun*. **2005**, 2995–3001.

[7] Moore, T.S.; Winmill, T.F. CLXXVII.-The State of Amines in Aqueous Solution. *J. Chem. Soc*. **1912**, *101*, 1635-1676.

[8] Latimer, W.M.; Rodebush, W. H. Polarity and Ionisation from the Standpoint of the Lewis Theory of Valence. *J. Am. Chem. Soc.* **1920,** *42*, 1419-1433

[9] Djafari, S.; Barth, H.-D.; Buchold, K.; Brutschy, B. J. Infrared-Depletion Spectroscopy Study on Hydrogen-Bonded Fluorobenzene-Methanol Clusters.*Chem. Phys*. **1997**, *107*, 10573-10581.

[10] Hobza, P.; Sponer, J.; Orozco, M.; Luque, F. J. Hydrogen Bond versus Anti-Hydrogen Bond: A comparative Analysis based on the Electron Density Topology. *J. Phys. Chem.***1999**, *103*, 6394-6401.

[11] Arunan, E.; Desiraju, G. R.; Kline, R. A.; Sadlej, J.; Schreiner, S.; Alkorta, I.; Clary, D.C.; Crabtree, R.H.; Dannenberg, J. J.; Hobza, P.; Kjaergaard, H. G.; Legon, A. C.; Mennucci B.; Nesbitt, D.J. Defination of Hydrogen Bond (IUPAC Recommendations). *Pure. Appl. Chem.* **2011,** *83*, 1637-1641.

[12] Desiraju, G.R.; Steiner, T. The Weak Hydrogen Bond in Structural Chemistry and Biology. **1999**, Oxford University Press Inc., New York.

[13] Steiner, S. Weak H-bonds. Comparisons of CH¨O to NH¨O in Proteins and PH¨N to Direct P¨N Interactions. *Phys. Chem. Chem. Phys*. **2011**, *13*, 13860–13872.

[14] Joseph, J.; Jemmis, E.D. Red-, Blue-, or No-Shift in Hydrogen Bonds: A Unified Explanation. *J. Am. Chem. Soc.* **2007**, *129*, 4620-4632.

[15] Saini J.; Viswanathan K.S. Discerning Near-Isoergic Isomers. A Matrix Isolation Infrared and *ab Initio* Study of the Propargyl Alcohol Dimers. *J. Phys. Chem. A.* **2017**, *121*, 1448−1459.

[16] Saini J.; Viswanathan K.S. Does a Hydrogen Bonded Complex with Dual Contacts show Synergism? A Matrix Isolation Infrared and *Ab Initio* Study of Propargyl Alcohol-Water Complex. *J. Mol. Struct.* **2016**, *1118*, 147-156.

[17] Engdahl, A.; Nelander, B. The Acetylene-WaterComplex. A Matrix Isolation Study. *Chem. Phys. Lett*. **1983**, *100*, 129-132

[18] Topol, I. A.; Tawa, G. J.; Caldwell, R. A., Eissenstat, M. A.; Burt, S. K. Acidity of Organic Molecules in the Gas Phase and in Aqueous Solvent. *J. Phys. Chem. A.* **2000,** *104*, 9619-9624.

[19] Karir, G.; Viswanathan, K. S. Phenylacetylene-Water Complex: Is it n···σ or H···π in the Matrix? *J. Mol. Struct.* **2016**, *1107*, 145-156.
[20]Whittle, E.; Dows, D.A.; Pimentel, G.C. *J. Chem. Phys.* Matrix Isolation Method for the Experimental Study of Unstable Species. **1954**, *22*, 1943.
[21] Norman, I.; Porter, G. Trapped Atoms and Radicals in a Glass 'Cage.'*Nature*, **1954**, *174*, 508-509.
[22] Goswami, M.; Arunan, E. Microwave Spectroscopic and Theoretical Studies on the Phenylacetylene...H_2O complex: C-H...O and O-H...π Hydrogen Bonds as Equal Partners. *Phys. Chem. Chem. Phys.* **2011**, *13*, 14153-14162.
[23] Sander, W.; Costa, P. Hydrogen Bonding Switches the Spin State of Diphenylcarbene from Triplet to Singlet. *Angew. Chem. Int. Ed.* **2014,** *53*, 1-5.
[24] Hobe, M. von; Stroh, F.; Beckers, H.; Benter, T.; Willner, H. The UV/Vis Absorption Spectrum of Matrix-Isolated Dichlorine Peroxide, ClOOCl. *Phys. Chem. Chem. Phys.* **2009**, *11*, 1571-1580.
[25] Moss,R. A; Platz, M.S; Hones, M; Reactive Intermediate Chemistry, John Wiley & Sons, **2004.**
[26] Sander, W.; Bücher, G.; and Wierlacher, S. Carbenes in Matrices- Spectroscopy, Structure, and Reactivity. *Chem. Rev.* **1993**, *93*, 1583-1621.
[27] Verma, K.; Dave, K.; Viswanathan, K. S. Hydrogen-Bonded Complexes of Phenylacetylene-Acetylene: Who is The Proton Donor ? *J. Phys. Chem. A.* **2015**, *119*, 126566-12664.
[28] Raut, A.; Karir, G.; Viswanathan, K.S. Matrix Isolation Infrared and *Ab Initio* Study of the Interaction of N-Heterocyclic Carbene with Water and Methanol: A Case Study of a Strong Hydrogen. *J. Phys. Chem. A.* **2016**.,120(47),9390-9400.
[29] Pimental, G.C; Charles, S.W; Infrared spectral perturbations in matrix experiments, Pure and Applied Chemistry, **1963**, *7*, 111-123.
[30] Nelander, B. An FTIR Study of Rotation of Ammonia in Solid Nitrogen. *J. Chem. Phys*. **1984**, *87*, 283-294.
[31] Robinson, D.W. Spectra of Matrix-Isolated Water in the "Pure Rotation" Region. *J. Chem. Phys.* **1963,** *39*, 3430-3432.
[32] Bowers, M.T.; Kerley, G.I.; Flygare, W.H. Vibration-Rotation Spectra of Monomeric HF in the Rare-Gas Lattices. *J. Chem. Phys.***1966**, *44*, 3399-3414.
[33] https://www.arscryo.com/cryocooler-principles-of-operation
[34] Xu S.; Chen, H.; Dai, J.; and Xu, H. Copper-Promoted Reductive Coupling of Aryl Iodides with 1,1,1- Trifluoro-2-iodoethane. *Org. Lett*. **2014**, *16*, 2306−2309.
[35] María I.; Rolando A. Electrogenerated Conductive Polymers from Triphenylamine Endcapped Dendrimers. *Macromolecules.* **2013**, *46*, 4754−4763.
[36] Frisch, M. J.; Trucks, G. W.; Schlegel, H. B.; Scuseria, G. E.; Robb, M. A.; Cheeseman, J. R.; Scalmani, G.; Barone, V.; Mennucci, B.; Peterson, G. A.; *et al*. GAUSSIAN 09, Revision C.01,Gaussian Inc., Wallingford CT, **2010**.
[37] Vincent, M. A.; Hillier, I. H. The Structure and Interaction Energies of the Weak Complexes of $CHClF_2$ and CHF_3 with HCCH: A Test of Density Functional Theory Methods. *Phys. Chem. Chem. Phys.* **2011**, *13*, 4388-4392.
[38] The Spectra were Simulated using SYNSPEC made Available by Irikura K., National Institute of Standards and Technology, Gaithesburg, MD 20899, USA, 1995.

[39] Turi, L.; Dannenberg, J. J. Molecular Orbital Studies of the Nitromethane-Ammonia Complex. An Unusually Strong CH…N Hydrogen Bond. *J. Phys. Chem*. **1995**, *99*, 639-641.
[40] Wong, N.B.; Cheung, Y.S; Wu, D. Y.; Ren, Y.; Wang, X.; Tian, A. M.; Li, W.K. A Theoretical Study of the C-H …N Hydrogen Bond in the Methane-Ammonia Complex. *J. Mol. Struct.* **2000**, *507*, 153-156.
[41] Boys, S. F.; Bernardi, F.The Calculation of Small Molecular Interactions by the Differences of Separate Total Energies.Some Procedures with Reduced Errors.*Mol. Phys.* **1970**, *19*, 553-566.
[42] Helgaker, T.; Klopper, W.; Koch, H.; Noga, J. Basis-Set Convergence of Correlated Calculations on Water. *J. Chem. Phys*. **1997**, *106*, 9639-9646.
[43] Bader R. F. W., Atoms in Molecules. A Quantum Theory, Clarendon Press, Oxford, **1994.**
[44] Blieger-König, F.; Bayles, D.; Schönbohn, J. AIM2000 (Version 1.0); Chemical Adviser: Bader, R. F. W.
[45] Koch, U.; Popelier,P. L. A. Characterization of C–H…O Hydrogen Bonds on the Basis of the Charge Density. *J. Phys. Chem.* **1995**, *99*, 9747-9754.
[46] Espinosa, E.; Molins, E.; Lecomte, C. Hydrogen Bond Strengths Revealed by Topological Analyses of Experimentally Observed Electron Densities. *Chem. Phys. Lett.* **1998**, *285*, 170-173.
[47] Glendening, E. D.; Carpenter, J. E.; Weinhold, F. NBO (Version 3.1)
[48] Boys, S. F.; Bernardi, F. The Calculation of Small Molecular Interactions by the Differences of Separate Total Energies.Some Procedures with Reduced Errors.*Mol. Phys.* **1970**, *19*, 553-566
[49] Stearns, J. A.; Zwier, T. S. Infrared and Ultraviolet Spectroscopy of Jet-Cooled ortho-, meta-, and para-Diethynylbenzene. *J. Phys. Chem. A.* **2003**, *107*, 10717-10724.
[50] Karir G.; Fatima, M.; Viswanathan K.S. The Elusive ≡C-H··O Complex in the Hydrogen Bonded Systems of Phenylacetylene: A Matrix Isolation Infrared and *Ab Initio* Study. *J. Chem. Sci*. **2016,** 128, 1557-1569.
[51] Delaat, A. M.; Ault, B. S. Infrared Matrix Isolation Study of Hydrogen Bonds Involving C-H Bonds : Alkynes with Oxygen Bases. *J. Am. Chem. Soc.* **1987**, *109*, 4232-4236.
[52] Schmidt, M. W.; Baldridge, K. K.; Boatz, J. A.; Elbert, S. T.; Gordon, M. S.; Jensen, J. H.; Koseki, S.; Matsunaga, N.; Nguyen, K. A.; Su, S., *et al.* General Atomic and Molecular Electronic Structure System. *J. Comp. Chem.* **1993**, *14*, 1347-1363.
[53] Karir, G. PhD Thesis "The Strange Case of Phenylacetylene : Competition between H-π and n-σ* Contacts Studied using Matrix Isolation Infrared Spectroscopy and *Ab Initio* Computations. 2018.